

RESEARCH ARTICLE

hnRNPH1 establishes Sertoli–germ cell crosstalk through cooperation with PTBP1 and AR, and is essential for male fertility in mice

Shenglei Feng^{1,*}, Hui Wen^{1,*}, Kuan Liu^{1,*}, Mengneng Xiong¹, Jinmei Li¹, Yiqian Gui¹, Chunyu Lv¹, Jin Zhang¹, Xixiang Ma^{1,2}, Xiaoli Wang¹ and Shuiqiao Yuan^{1,2,3,‡}

ABSTRACT

Spermatogenesis depends on the crosstalk of Sertoli cells (SCs) and germ cells. However, the gene regulatory network establishing the communications between SCs and germ cells remains unclear. Here, we report that heterogeneous nuclear ribonucleoprotein H1 (hnRNPH1) in SCs is essential for the establishment of crosstalk between SCs and germ cells. Conditional knockout of hnRNPH1 in mouse SCs leads to compromised blood–testis barrier function, delayed meiotic progression, increased germ cell apoptosis, sloughing of germ cells and, eventually, infertility of mice. Mechanistically, we discovered that hnRNPH1 could interact with the splicing regulator PTBP1 in SCs to regulate the pre-mRNA alternative splicing of the target genes functionally related to cell adhesion. Interestingly, we also found hnRNPH1 could cooperate with the androgen receptor, one of the SC-specific transcription factors, to modulate the transcription level of a group of genes associated with the cell–cell junction and EGFR pathway by directly binding to the gene promoters. Collectively, our findings reveal a crucial role for hnRNPH1 in SCs during spermatogenesis and uncover a potential molecular regulatory network involving hnRNPH1 in establishing Sertoli–germ cell crosstalk.

KEY WORDS: hnRNPH1, Sertoli cells, Alternative splicing, Spermatogenesis, Mouse

INTRODUCTION

Mammalian spermatogenesis is a complex physiological process of sperm production in the testicular seminiferous tubules, which is supported by intricate crosstalk between Sertoli cells (SCs) and germ cells (Neto et al., 2016). Meiotic and post-meiotic germ cell development is confined to a specialized microenvironment within the seminiferous epithelium, and a key determinant of such a microenvironment is the formation of specialized tight junctions between SCs (Mruk and Cheng, 2015; Stanton, 2016). These specialized junctions form the basis of the blood–testis barrier (BTB), which comprises adherents, gap and occluding junctions

interspersed with tubulobulbar complexes (TBCs) and actin-based SC cytoskeletal structures (Dunleavy et al., 2019; Vogl et al., 2008). BTB divides the seminiferous epithelium into the basal and the apical (adluminal) compartments, and prevents the free passage of substances into the adluminal compartment of the seminiferous tubules (Chen et al., 2016a).


Increasing studies focus on the biology of the BTB because a complete loss of BTB function leads directly to infertility (Mao et al., 2020). BTB formation coincides with the increases in serum gonadotropins during puberty, such as follicle-stimulating hormone (FSH), luteinizing hormone (LH) and androgens (Stanton, 2016). Tight junction formation can be prevented by the removal of these hormones (Bressler, 1976). Androgens are mainly secreted by Leydig cells upon LH stimulation and act directly on receptors found in SCs to promote spermatogenesis (McLachlan et al., 2002; O’Shaughnessy, 2014). Previous studies have demonstrated that androgens can stimulate the mRNA expression, protein production and localization of tight junction proteins into the BTB (Stanton, 2016). The finding that androgen action was essential for BTB function *in vivo* was confirmed via a mouse model in which the androgen receptor (AR) in the SC was knocked out (Meng et al., 2005; Smith and Walker, 2014; Willems et al., 2010). As a transcription factor, AR regulates its activity by forming different splicing variants that are mediated by several splicing factors, such as PTBP1 (also known as hnRNPI) (Liu et al., 2014). Interestingly, PTBP1 was also reported to maintain the integrity of the BTB by regulating the expression levels of tight junction-associated proteins (Yang et al., 2021). However, the underlying molecular networks among PTBP1 and AR in SCs for the regulation of BTB and spermatogenesis are poorly understood.

RNA-binding proteins (RBPs) are key components in RNA metabolism that play crucial roles in the post-transcriptional control of RNAs, including splicing, mRNA stability, mRNA localization, polyadenylation and translation (Bataclan et al., 2021). Heterogeneous nuclear ribonucleoproteins (hnRNPs) are a large family of RNA binding proteins with crucial roles in multiple aspects of RNA metabolism as well. Several members of the hnRNP family were reported to be highly expressed in male germ cells and SCs and involved in the process of spermatogenesis (Li et al., 2012; Wen et al., 2021; Xu et al., 2018). Among the hnRNP family members, hnRNPH1 has attracted increasing public attention based on its critical function in neurological diseases and cancers (Prudencio et al., 2015; Uren et al., 2016; Wu et al., 2021). Notably, our recent study showed that hnRNPH1 could recruit the splicing factors PTBP2 and SRSF3 to regulate alternative splicing in germ cells (Feng et al., 2022). However, the

¹Institute of Reproductive Health, Tongji Medical College, Huazhong University of Science and Technology, Wuhan 430030, China. ²Laboratory of Animal Center, Huazhong University of Science and Technology, Wuhan 430030, China. ³Shenzhen Huazhong University of Science and Technology Research Institute, Shenzhen, Guangdong 518057, China.

*These authors contributed equally to this work

‡Author for correspondence (shuiqiaoyuan@hust.edu.cn)

 H.W., 0000-0001-6238-8758; S.Y., 0000-0003-1460-7682

Handling Editor: Haruhiko Koseki

Received 20 June 2022; Accepted 3 January 2023

physiological role and potential mechanism of hnRNPH1 in SCs on spermatogenesis and male fertility remain elusive.

Here, we show that the hnRNPH1 protein is highly expressed in mouse SCs and is indispensable for spermatogenesis and male fertility. The loss of function of hnRNPH1 in mouse SCs leads to complete male infertility, characterized by not only severe destruction of the structure and function of the BTB but also by impaired meiotic processes. We further discovered that hnRNPH1 could interact with the splicing regulator PTBP1 to regulate the alternative splicing of its target genes that are functionally related to cell adhesion in SCs. In addition, we found that hnRNPH1 in SCs could also cooperate with the AR, one of the SC-specific transcription factors, to modulate gene transcription by directly binding their promoter. Our data, for the first time, identify a previously unreported role for hnRNPH1 in SCs on spermatogenesis and male fertility. Furthermore, our data uncovered a molecular regulatory network of hnRNPH1 in SCs through cooperation with the splicing factor PTBP1 and the transcription factor AR to regulate pre-mRNA alternative splicing and gene transcription in SCs.

RESULTS

hnRNPH1 is highly expressed in SCs through pre-pubertal to adult mouse testis

To explore the functions of hnRNPH1 in spermatogenesis, we first examined its expression pattern in adult mouse testes through immunofluorescence (IF) assays. The results showed that hnRNPH1 is highly expressed in SCs because of the significant colocalization with WT1 (an SC marker) in testes and purified SCs (Fig. 1A,B). In addition, hnRNPH1 is expressed in germ cells, especially in spermatocytes and round spermatids (Fig. 1A). Furthermore, IF analyses revealed that hnRNPH1 is continuously expressed in SCs at different developmental stages (Fig. 1C); however, its expression level is relatively low in the early stages

from embryonic day 17.5 (E17.5) to postnatal day 7 (P7), suggesting that hnRNPH1 may play a crucial role in SCs at multiple stages of germ cell development.

hnRNPH1 in SCs is required for spermatogenesis and male fertility

Given the strong expression of hnRNPH1 in SCs, we speculate that hnRNPH1 in SCs may play a role in spermatogenesis. To test this hypothesis, we generated SC-specific conditional knockout (cKO) mice by crossing *Hnrnp1*^{flx/flx} mice with the *Amh-Cre* transgenic mouse strain to investigate the function of hnRNPH1 in SCs on spermatogenesis. A *Hnrnp1*-null allele in SCs was created after *Amh-Cre*-mediated recombination of the floxed-*Hnrnp1* allele with LoxP sites flanking exon 6 (Fig. S1A), and the conditional knockout (*Amh-Cre; Hnrnp1*^{flx/flx}; hereafter referred to as hnRNPH1 cKO) and control (*Hnrnp1*^{flx/flx} or *Hnrnp1*^{+ /flx}; *Amh-Cre*; hereafter referred to as control) mice were verified through PCR-based genotyping with indicated primers (Fig. S1B). Both mRNA and protein levels of hnRNPH1 were almost absent in the purified hnRNPH1 cKO SCs compared with the control (Fig. 2A,B). Furthermore, co-staining of hnRNPH1 with WT1 in control and hnRNPH1 cKO testis sections at P56 further confirmed a specific ablation of hnRNPH1 in the hnRNPH1 cKO SCs (Fig. 2C). These data indicate that, in the hnRNPH1 cKO male mice, the *Hnrnp1* gene was successfully deleted in SCs.

After fecundity testing for 6 months, the control males produced 8.2 pups per cage, whereas the hnRNPH1 cKO males never produced any pups (Fig. 2D), suggesting the hnRNPH1 cKO males are completely infertile. In addition, the testis size of hnRNPH1 cKO mice was significantly smaller than that of controls (Fig. 2E), and the ratio of testis weight/body weight of hnRNPH1 cKO mice was obviously reduced compared with controls from P21 onwards (Fig. 2F). Consistent with this result, histological analyses of developing testes showed that the diameter of seminiferous tubules

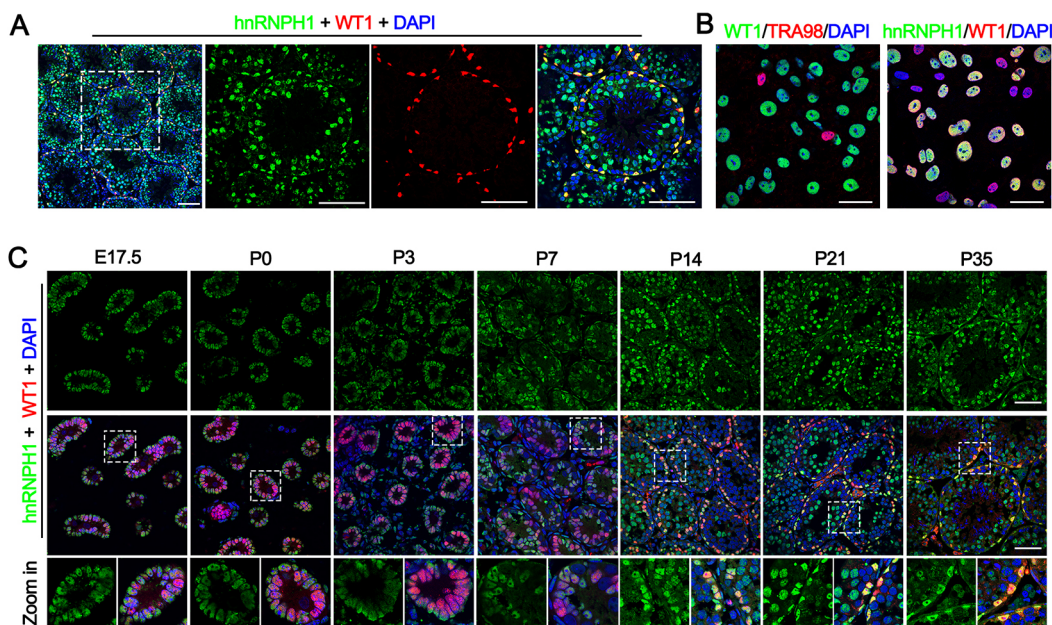


Fig. 1. hnRNPH1 localizes in mouse SCs. (A) Anti-hnRNPH1 and anti-WT1 antibodies (an SC marker) were used to double immunostain wild-type adult testicular cryosections. Scale bars: 50 μ m. (B) The purity of the isolated SCs from wild-type P21 testes was determined by the immunofluorescence co-staining of WT1 and TRA98. Anti-hnRNPH1 and anti-WT1 antibodies were used for double immunostaining of purified SCs from wild-type P21 testes. Scale bars: 20 μ m. (C) Double immunostaining with hnRNPH1 and WT1 on testicular cryosections from wild-type mice at different ages. Scale bars: 50 μ m.

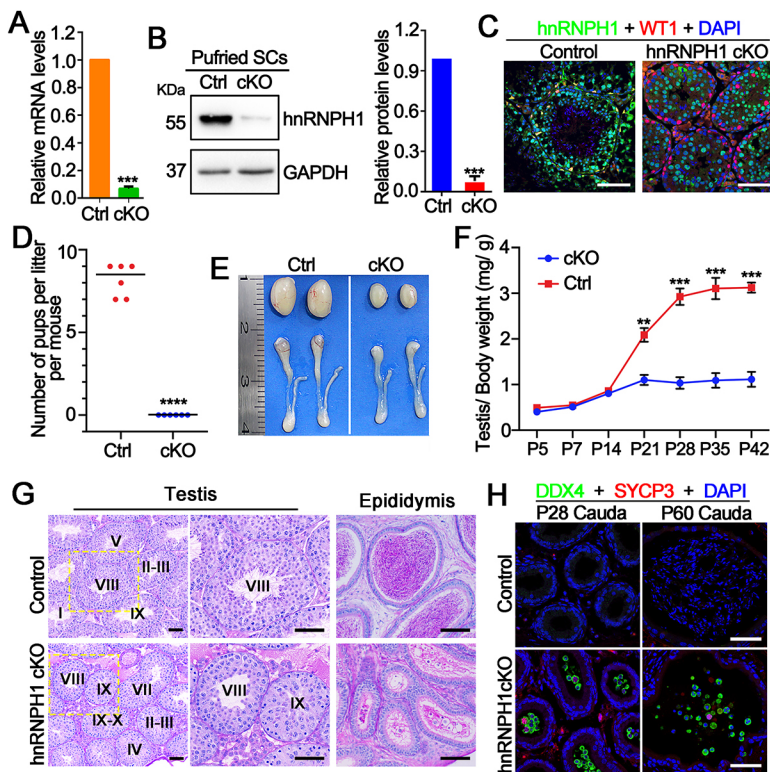


Fig. 2. Conditional knockout of hnRNPH1 in SCs results in severe obstruction of spermatogenesis and male infertility. (A,B) RT-qPCR (A) and western blot (B) analyses of *HnRNPH1* expression levels in SCs isolated from control and hnRNPH1 cKO mouse testes. Data are mean±s.e.m., $n=3$. *** $P<0.001$ (unpaired Student's *t*-test). GAPDH served as a loading control. (C) Representative co-immunofluorescent images of hnRNPH1 (green) and WT1 (red) in adult control and hnRNPH1 cKO testis cryosections. Scale bars: 50 μ m. (D) The average numbers of pups per litter produced from control and hnRNPH1 cKO male mice. Data are mean±s.e.m., $n=6$. **** $P<0.0001$ (unpaired Student's *t*-test). (E) Gross morphology of the testes and epididymides from adult control and hnRNPH1 cKO male mice. (F) Testis growth curves from control and hnRNPH1 cKO mice at different ages. Data are mean±s.e.m., $n=3$. ** $P<0.01$ and *** $P<0.001$ (unpaired Student's *t*-test). (G) Periodic acid-Schiff (PAS) staining showing the histology of testes and epididymides sections from adult control and hnRNPH1 cKO male mice. Scale bars: 50 μ m. (H) Anti-DDX4 and anti-SYCP3 antibodies were used to double immunostain cauda from control and hnRNPH1 cKO mice at P28 (left) and P60 (right). Scale bars: 50 μ m.

was decreased in hnRNPH1 cKO mice compared with that of control mice from P21 onwards (Fig. S1C). Further histological analyses of adult testes showed that, in control males, the various stages of spermatogenic cells were observed in seminiferous tubules (Fig. 2G and Fig. S1D), whereas in hnRNPH1 cKO males, there were no detectable mature spermatozoa in seminiferous tubules and cauda epididymis (Fig. 2G), and spermatogenesis was arrested in step 15 spermatids (Fig. S1E). Furthermore, quantitative analysis revealed a significant decrease in spermatocytes or spermatids in the adult hnRNPH1 cKO mice (Fig. S1F). The TUNEL assay revealed that the number of apoptotic cells in hnRNPH1 cKO testes was much more than that of controls even at the early P14 stage (Fig. S1G), suggesting dystrophy of the developing spermatocytes during the first wave of spermatogenesis. Of note, a large number of round spermatids and a few spermatocytes were found to be prematurely sloughed into cauda epididymis at P28 and P60 (Fig. 3H). We then examined the development of germ cells and SCs in the perinatal period because hnRNPH1 was expressed in SCs as early as the embryonic stage. Interestingly, we found that the numbers of germ cells (TRA98⁺) and SCs (WT1⁺) are comparable between control and hnRNPH1 cKO testes (Fig. S2A,B). Moreover, the hnRNPH1 deficiency does not affect the development and differentiation of spermatogonia both in juvenile and adult mice (Fig. S2C-F). Together, these results indicate that hnRNPH1 in SCs is essential for late spermatogenesis in mice and that ablation of hnRNPH1 in SCs results in male sterility.

hnRNPH1 interacts with PTBP1 and AR in SCs

To explore the underlying molecular mechanism of hnRNPH1 in SCs regulating spermatogenesis, a combined immunoprecipitation-mass spectrometry (IP-MS) approach was applied to identify the interactome of hnRNPH1 in purified SCs. Consequently, a total of 128 proteins were identified from the immunoprecipitates,

including hnRNPH1 itself (Fig. 3A and Table S1). Gene ontology (GO) and KEGG enrichment analyses indicated that these proteins are functionally most related to 'mRNA splicing' and 'Spliceosome' (Fig. 3B). Interestingly, among the 20 hnRNPH1-interacting proteins screened by the STRING database (Fig. S3A), three key splicing factors [PTBP1 (Yang et al., 2021), SFPQ (Knott et al., 2016) and NONO (Dong et al., 2017)] and a transcription factor [androgen receptor, AR (Willems et al., 2010)] have been reported to be highly expressed in SCs and involved in spermatogenesis. Thus, we focused on these four candidate proteins for further investigation. Co-immunoprecipitation (co-IP) and GST-pull down assays demonstrated that both PTBP1 and AR interact with hnRNPH1 in the purified SCs (Fig. 3C and Fig. S3B), whereas the interaction of SFPQ and NONO with hnRNPH1 seemed to depend on RNA or DNA (Fig. S3C). In addition, an apparent colocalization of hnRNPH1 with PTBP1 and AR was observed in the SC nucleus (Fig. S3D,E), further supporting the potential cooperation of hnRNPH1 with PTBP1 and AR in the SCs. Notably, the expression and localization of PTBP1 and AR were not affected upon hnRNPH1 ablation (Fig. S3D,E). Interestingly, similar to hnRNPH1, both AR and PTBP1 began to be highly expressed in SCs from the P14 stage but displayed lower expression in earlier stage SCs from E17.5 to P7 testes (Fig. S3F,G). To further understand the potential mechanism by which hnRNPH1 interacts with PTBP1 and AR *in vitro*, their direct association was checked via ectopic co-expression of hnRNPH1, PTBP1 and AR in HEK293T cells. Reciprocal co-IP assays revealed that hnRNPH1 could directly bind PTBP1 and AR (Fig. 3D-G). It was further found that the 1-100 amino acid region (containing the qRRM1 domain) of hnRNPH1 and the 623-685 amino acid region (containing the Hinge domain) of AR was responsible for the interaction between hnRNPH1 and AR (Fig. 3D,E); the 200-288 amino acid region (containing the GRY domain) of hnRNPH1 and the 50-180 amino acid region (containing the RRM1 domain) of

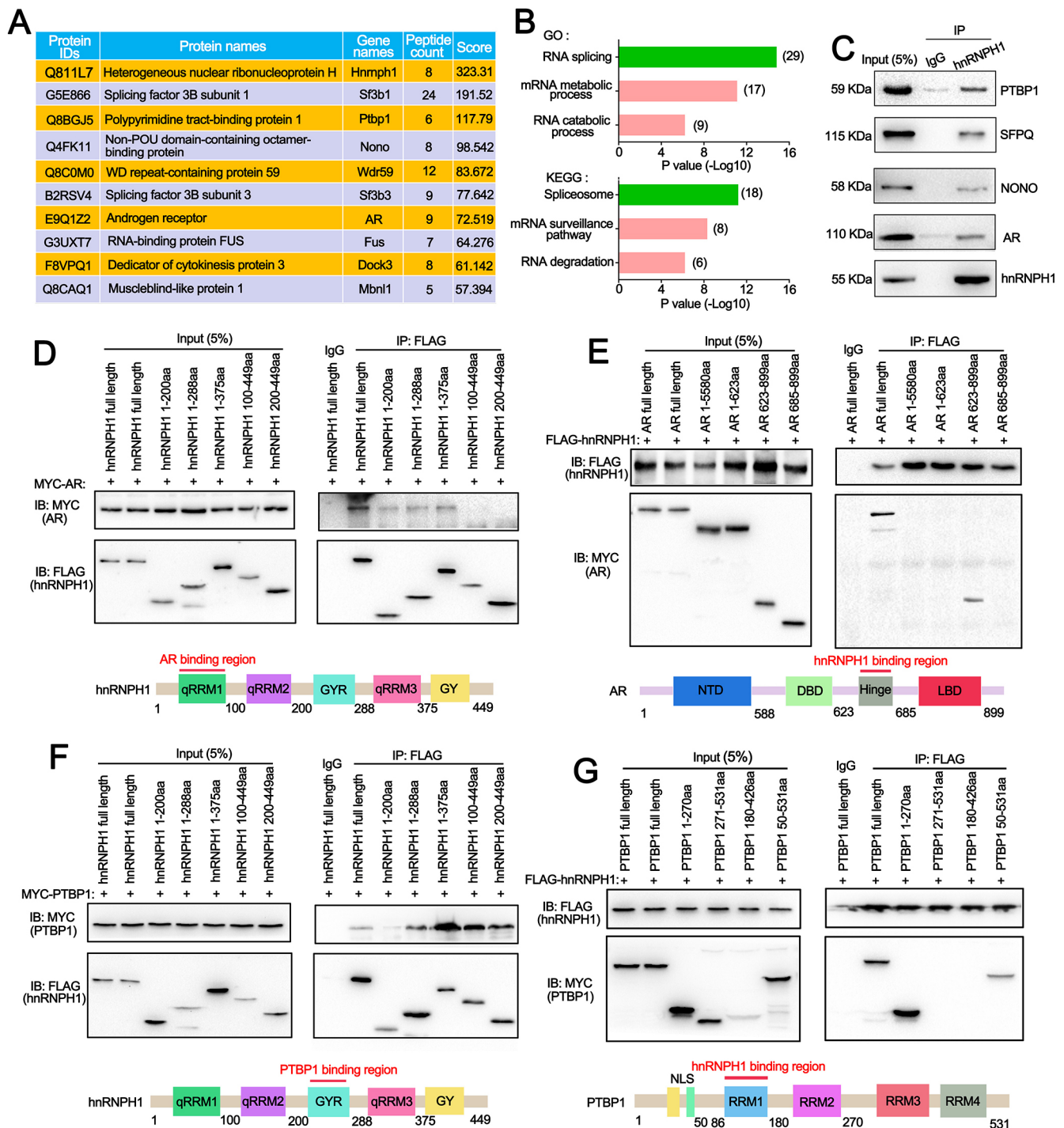


Fig. 3. hnRNPH1 interacts with PTBP1 and AR in SCs. (A) A list of 10 hnRNPH1-interacting partners in purified SCs from wild-type testes at P21 identified by immunoprecipitation-mass spectrometry (IP-MS). (B) GO (upper) and KEGG (lower) term enrichment analyses show the hnRNPH1-interacting proteins identified from IP-MS data. (C) Validation of interactions between hnRNPH1 and four putative hnRNPH1-interacting proteins (PTBP1, SFPQ, NONO and AR) in purified SCs by co-IP assays. IgG was used as a negative control. (D-G) Reciprocal co-IP assays of interaction domains between hnRNPH1 and its binding partners AR and PTBP1. HEK293T cells were co-transfected with MYC-AR and the indicated fragments of FLAG-hnRNPH1 (D), co-transfected with FLAG-hnRNPH1 and the indicated fragments of MYC-AR (E), co-transfected with MYC-PTBP1 and the indicated fragments of FLAG-hnRNPH1 (F), or co-transfected with FLAG-hnRNPH1 and the indicated fragments of MYC-PTBP1 (G), immunoprecipitated with anti-FLAG antibody, and immunoblotted with FLAG and MYC antibodies, respectively.

PTBP1 were essential for the interaction between hnRNPH1 and PTBP1 (Fig. 3F,G). Altogether, these data suggest that hnRNPH1 cooperates with transcription factor AR and mRNA splicing factors PTBP1 in mouse SCs through specific regions.

Ablation of hnRNPH1 in SCs results in disruption of BTB and meiosis

Considering that PTBP1 and AR have been reported to regulate spermatogenesis and that a common phenotype in their knockout

mice was the abnormal BTB function (Willems et al., 2010; Yang et al., 2021), we decided to clarify whether the BTB integrity was abolished in hnRNPH1 cKO mouse testes. BTB is a specialized cell junction between SCs that is composed of tight junction (TJ), basal ectoplasmic specialization (ES) and a gap junction (Wen et al., 2018). An IF assay showed that, in control testes, the basal TJ proteins (N-cadherin and β -catenin) and ES proteins (ZO-1) were localized in the basal membrane of seminiferous tubules (Fig. 4A and Fig. S4A). In contrast, in hnRNPH1 cKO testes, these proteins were found to be beyond the basement membrane and diffusely present at the BTB, extending towards the lumen (Fig. 4A and Fig. S4A). As the BTB structures are supported by the concerted efforts of the microtubule- and actin-based cytoskeletons (Dunleavy et al., 2019), we examined whether the cytoskeletons of SCs were affected in the hnRNPH1 cKO testes. Consequently, immunostaining of α -tubulin and F-actin revealed disruption of microtubular arrangement and actin organization in the hnRNPH1 cKO SCs (Fig. 4B,C). Thereafter, the BTB integrity was further detected by biotin tracing assay *in vivo*, and the results showed that the biotin tracer could permeate into seminiferous tubules in the hnRNPH1 cKO testes; this was similar to observations made in the positive control after treatment with cadmium chloride (CdCl₂), which is known to have destructive effects on the BTB (Jia et al., 2017) (Fig. 4D-F). Furthermore, ultrastructural analysis by transmission electron microscopy (TEM) revealed an intact BTB structure in control seminiferous tubules (Fig. S4B); by contrast, an abnormal SC morphology and BTB structure with large irregular cavities was observed in the hnRNPH1 cKO seminiferous epithelium. These data indicate that ablation of hnRNPH1 in SCs compromises the BTB integrity of SCs. In addition, we found that the length of vimentin (a cytoskeleton marker in the cytoplasm of SCs) filaments of SCs in hnRNPH1 cKO seminiferous tubules is shorter than that of controls (Fig. 4G,H), which suggests that the destruction of BTB may be attributed to the abnormal development of SCs with disorganized cytoskeleton due to ablation of hnRNPH1 in SCs. To explore whether the apical ES is affected upon hnRNPH1 depletion in SCs, F-actin staining was conducted in control and hnRNPH1 cKO mouse testis. As shown in Fig. 4I, F-actin is disorganized in hnRNPH1 cKO seminiferous tubules, and the structure of apical ES is also disrupted. Considering that disruption of BTB function is related to the appearance of many immune cells in the testes (Qu et al., 2020), we then tested this by immunostaining for the macrophage marker CD68 and the T-cell marker CD8. The results revealed a significant increase in the number of immune cells in the hnRNPH1 cKO testicular interstitial regions compared with controls (Fig. S4C), suggesting that the disruption of BTB function in hnRNPH1 cKO testes may cause an imbalance in the immune barrier of the testicular microenvironment.

Given that AR deficiency in mice causes abnormal meiosis (Chen et al., 2016b), we next asked whether hnRNPH1 ablation in SCs affects the meiotic process by chromosome spreading analyses. As shown in Fig. 4J, in control pachytene spermatocytes, γ H2AX signals completely disappear from autosomes but are confined to the XY bodies formed by sex chromosomes. However, a higher proportion of hnRNPH1 cKO spermatocytes (48.5% in cKO versus 2.9% in control) displayed an abnormal γ -H2A.X distribution from controls (Fig. 4K), indicating the DNA damage response remained active in synapsed homologs of hnRNPH1 cKO spermatocytes. This conclusion was further verified by immunostaining of RPA (a DNA recombination marker), which showed abnormal DSB repair in the hnRNPH1 cKO pachytene spermatocytes (Fig. 4L,M). In addition, the hnRNPH1 cKO spermatocytes exhibited

developmental retardation because of a lower proportion of pachytene and diplotene spermatocytes than controls (Fig. 4N). A similar result was found from the staining of HIT (a mid-late pachytene marker) (Fig. 4O,P). These data reveal that hnRNPH1 ablation in SCs can impair the meiotic process.

hnRNPH1 in SCs regulates mRNA alternative splicing through cooperation with PTBP1

Previous studies have elucidated the role of hnRNPH1 in the regulation of pre-mRNA splicing (Uren et al., 2016). Interestingly, we identified numerous hnRNPH1-interacting partners in this study, and many of them were splicing factors, such as PTBP1; thus, we speculated that hnRNPH1 is likely involved in regulating pre-mRNA alternative splicing (AS) in SCs. To test this, high-purity SCs from P21 hnRNPH1 cKO and control testes were isolated, and total RNA was extracted and processed using high-throughput RNA-seq analysis. As expected, the RNA-seq analysis identified 110 aberrant mRNA alternative splicing events in hnRNPH1 cKO purified SCs (Table S2), including skipped exons (SE), alternative 5' splice sites (A5SS), alternative 3' splice sites (A3SS), mutually exclusive exons (MXE) and retained introns (RI) (Fig. 5A; $|\Delta\text{PSI}| > 10\%$, $P < 0.05$), affecting a total of ~92 genes. Approximately 59.1% and 40.9% of AS events were found to be upregulated and downregulated in hnRNPH1 cKO purified SCs, respectively (Fig. 5B). Among the aberrant AS events affected by hnRNPH1 deletion, SE is the predominant splicing type (40.9%) (Fig. 5C). Interestingly, GO term analysis of these abnormal AS event-involved genes revealed enrichment of functional categories related to 'cell-cell junction maintenance' and 'actin cytoskeleton organization' (Fig. 5D), which may explain the phenotype of compromised BTB function in hnRNPH1 cKO testes. We then examined the splicing levels of corresponding exons of those genes to determine whether they were altered in hnRNPH1 cKO purified SCs by RT-PCR analysis. The results confirmed that eight out of 12 tested genes displayed abnormal mRNA splicing in the hnRNPH1-null SCs (Fig. 5E and Fig. S5A). Furthermore, western blot results revealed a significant change in protein levels of some of these abnormal AS event-involved genes (e.g. *Espn*, *Pard6a*, *Atp1a1* and *Hgf*) in hnRNPH1-deficient SCs, compared with controls (Fig. 5F and Fig. S5B). Consistent with this result, IF assays also showed reduced fluorescence signal for ESPN and PARD6A in the hnRNPH1 cKO testis sections (Fig. 5G,H). Combined with the previous reports that these abnormal AS event-involved genes identified in this study, *Espn* (Chen et al., 1999), *Pard6a* (Wong et al., 2008), *Atp1a1* (Rajamanickam et al., 2017) and *Hgf* (Catizone et al., 2008) have been found to be involved in maintenance of BTB integrity, our data indicate that the aberrant mRNA alternative splicing of these four genes in hnRNPH1-deficient SCs leads to impaired BTB integrity and impaired communication between SCs and germ cells.

Because hnRNPH1 is expressed in embryonic and neonatal SCs (Fig. 1C), we asked whether any similar effect on splicing events occurs in the early stages. To this end, we first examined the mRNA expression of these target genes in isolated SCs of various stages by RT-PCR. Interestingly, we found that these target genes are almost not expressed in the E17.5 and P0 testes, and some of these target genes (e.g. *Efemp1*, *Pard6a*, *Kifc3* and *Tnnt1*) begin to express in testes from P7 onwards (Fig. S5C). We then checked their alternative splicing in isolated SCs from P7 to P21 and found that these genes display abnormal splicing in hnRNPH1 cKO SCs of P14 and P21 but not P7 testes (Fig. S5D). To clarify whether the homologous proteins of hnRNPH1, such as hnRNPF and

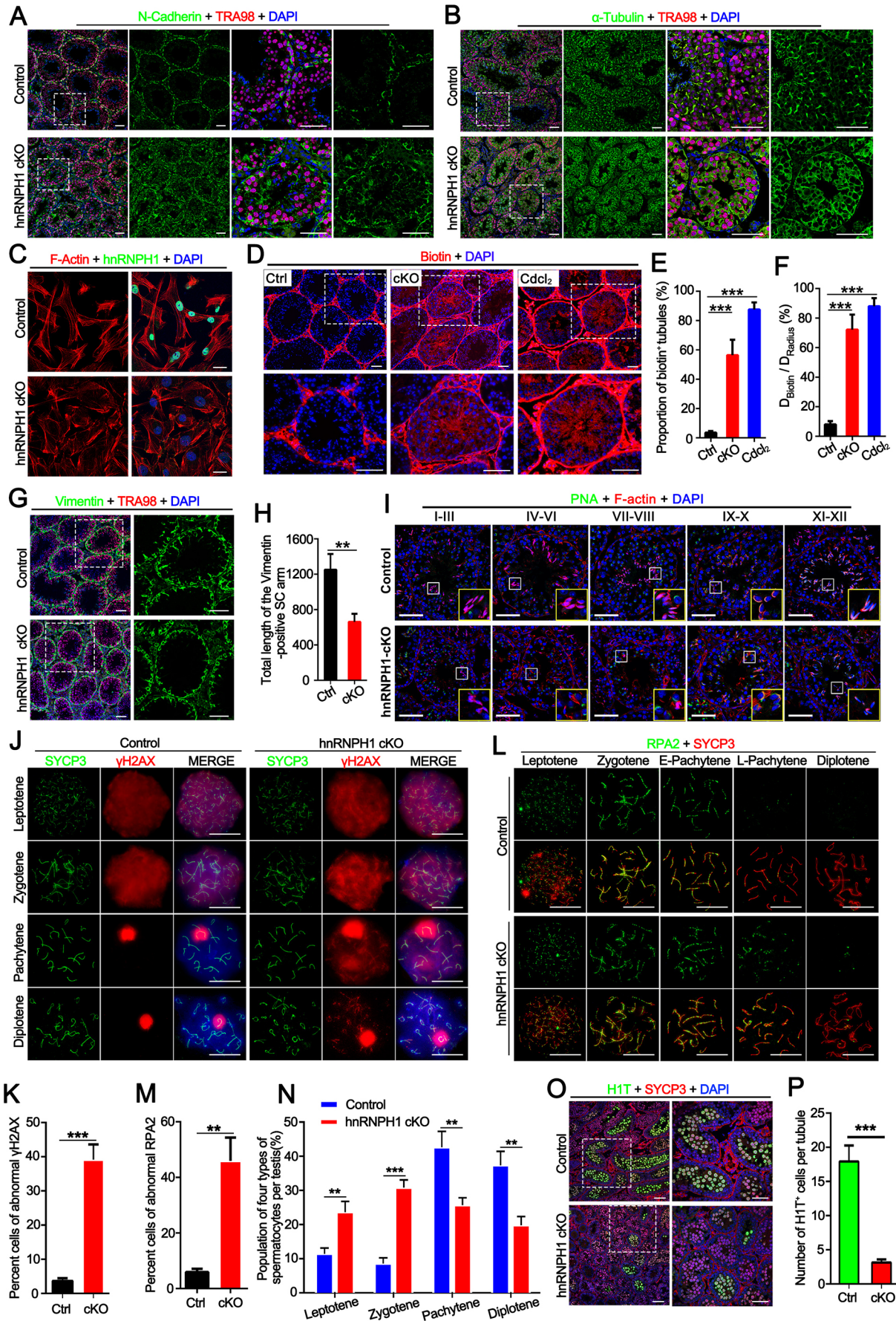


Fig. 4. See next page for legend.

Fig. 4. Ablation of hnRNPH1 in SCs results in severe disruption of the cytoskeleton and aberrant meiosis. (A,B) Co-immunofluorescence staining of TRA98 and either N-cadherin (A) or α -tubulin (B) in adult control and hnRNPH1 cKO testes. Scale bars: 50 μ m. (C) Co-immunofluorescence staining of hnRNPH1 and F-actin in adult control and hnRNPH1 cKO testes. Scale bars: 20 μ m. (D) The appearance of biotin tracer dye in the adluminal compartment of seminiferous tubules of adult hnRNPH1 cKO mice suggests a leaky BTB, whereas control mice show restriction of the biotin tracer to the basal compartment. As a positive control, mice were treated with a single dose of CdCl₂ at 5mg/kg 3 days before a BTB integrity assay. Scale bars: 50 μ m. (E,F) Histograms illustrating results of the BTB integrity assay. The permeability of the BTB was semi-quantified by the ratio of diffusion distance of the biotin tracer (D_{Biotin}) and the radius of the corresponding tubule (D_{radius}). Data are mean \pm s.d. of 100 tubules randomly selected from three mice. *** P <0.001 (one-way ANOVA). (G) Co-immunofluorescence staining of TRA98 and vimentin in adult control and hnRNPH1 cKO testes. Scale bars: 50 μ m. (H) Quantification of vimentin-positive cell arms in G. The total length of the vimentin-positive SC arm shows the sum of all cytoplasmic vimentin signals reaching from the basal membrane up to the tubular lumen in vimentin-stained testicular sections. Data are mean \pm s.d., n =3, ** P <0.01 (unpaired, two-tailed Student's t -test). (I) Co-immunofluorescence staining of PNA and F-actin at different stages for adult control and hnRNPH1 cKO testes. Scale bars: 50 μ m. (J) Co-immunofluorescence staining of SYCP3 with γ H2AX in spermatocyte spreads from control and hnRNPH1 cKO mice. Scale bars: 5 μ m. (K) Percentages of abnormal γ H2AX distribution at the pachytene stage in the control and hnRNPH1 cKO male mice. Data are mean \pm s.d., n =3, *** P <0.001 (unpaired Student's t -test). (L) Co-immunofluorescence staining of SYCP3 with RPA2 in spermatocyte spreads at the leptotene, zygotene, early-pachytene (E-pachytene), late-pachytene (L-pachytene) and diplotene stages from control and hnRNPH1 cKO male mice. Scale bars: 5 μ m. (M) Percentages of abnormal RPA2 distribution at the pachytene stage in the control and hnRNPH1 cKO male mice. Data are mean \pm s.d., n =3, ** P <0.01 (unpaired Student's t -test). (N) Percentages of spermatocytes at the leptotene, zygotene, pachytene and diplotene stages in the control and hnRNPH1 cKO mice. Data are mean \pm s.e.m., n =3, *** P <0.01, *** P <0.001 (unpaired Student's t -test). (O) Co-immunofluorescence staining of H1T and SYCP3 in control and hnRNPH1 cKO testes at P15. Scale bars: 50 μ m. (P) Quantification of H1T-positive cells per tubule for O. Data are mean \pm s.e.m., n =3, *** P <0.001 (unpaired, two-tailed Student's t -test).

hnRNPH2, can compensate for the deficiency of hnRNPH1 in SCs, we examined their expression levels in postnatal and adult stage SCs. As shown in Fig. S5E-I, the mRNA and protein levels of hnRNPF and hnRNPH2 in SCs were not affected during these periods after hnRNPH1 deletion. Similarly, the expression of the hnRNPH1-related proteins AR and PTBP1 in the hnRNPH1 cKO SCs was also unchanged (Fig. S5J-L). Given that hnRNPH1 was found to interact with the splicing factor PTBP1 in SCs, we next sought to determine whether there is a cooperation between hnRNPH1 and PTBP1 in the regulation of pre-mRNA alternative splicing in SCs. A RNA immunoprecipitation (RIP) assay was performed using the anti-hnRNPH1 and anti-PTBP1 antibodies to immunoprecipitate the pre-mRNAs from purified SCs. Eight genes with proven abnormal mRNA splicing in hnRNPH1-deficient SCs were chosen for qPCR analyses. The results showed that four genes (*Kifc3*, *Tnnt1*, *Espn* and *Pard6a*) were enriched both in hnRNPH1 and in PTBP1 immunoprecipitates (Fig. 5I). Thereafter, the knockdown experiments were performed in HEK293T cells *in vitro* to check whether PTBP1 could regulate the above four genes at the splicing level. Interestingly, the alternative splicing of three genes (*Kifc3*, *Espn* and *Pard6a*) was found to have changed in the same direction when hnRNPH1 and PTBP1 were knocked down (Fig. 5J). Furthermore, the binding affinity of these three target genes to PTBP1 was tested by RIP-qPCR assay in control and hnRNPH1 cKO SCs. The result showed that the enrichment level of these three genes bound to PTBP1 protein significantly decreased in

hnRNPH1-deficient SCs compared with control (Fig. 5K-M). These data suggest that hnRNPH1 could recruit PTBP1 and cooperatively regulate the mRNA alternative splicing of its target genes.

hnRNPH1 in SCs regulates gene transcription by modulating AR activity

In addition to the spliced genes, many differentially expressed genes (DEGs) were found in hnRNPH1 cKO SCs from the RNA-seq data (Table S3). Hierarchical clustering of DEGs showed that 305 genes were upregulated and 106 genes were downregulated (P ≤0.05, fold change≥2) in hnRNPH1-deficient SCs compared with control (Fig. 6A). Further GO term enrichment analyses revealed that the upregulated genes were mainly members of categories related to 'cell-cell adhesion' and 'cytoskeleton organization', and the downregulated genes were members of categories related to 'cell junction organization', 'cell adhesion molecules' and 'cell-substrate adhesion' (Fig. 6B,C), which are consistent with the phenotypic and functional results of hnRNPH1 cKO mice. Of note, among the GO terms, the 'retinoic acid metabolic process' was also reported to regulate the BTB structure (Hasegawa and Saga, 2012). We then chose some differentially expressed genes mainly related to cell adhesion and retinoic acid metabolism to perform RT-qPCR assays, and the results were almost consistent with the RNA-seq data (Fig. 6D,E and Fig. S5B). Interestingly, some of these 'cell junction' genes are directly associated with the regulation of BTB function, such as *Sox8* (Singh et al., 2013), *Krt18* (Setthawong et al., 2019), *Pkp2* (Li et al., 2009), *Itga6* (Wang et al., 2016), *Lcp1* (Lv et al., 2020) and *Cldn5* (Morrow et al., 2009). Western blots were performed to examine whether the protein expression of these crucial genes is affected in hnRNPH1-deficient SCs. The results showed that, compared with the control groups, the protein levels of KRT18, PKP2 and ITGA6 in hnRNPH1 cKO SCs decreased, while the levels of CLDN5 and LCP1 increased (Fig. 6F and Fig. S6A). In addition, IF analysis further revealed abnormal distribution and reduced expression of KRT18 and PKP2 in hnRNPH1 cKO testis sections compared with controls (Fig. 6G,H). These data indicate that hnRNPH1 ablation in SCs could affect the gene expression at both transcriptional and post-transcriptional levels in SCs.

Notably, we identified that many DEGs are involved in retinoic acid metabolism and the EGFR pathway from our RNA-seq datasets (Table S3 and Fig. S6B,C). As AR was identified as an hnRNPH1-interacting partner in SCs in this study and has previously been reported to control the meiotic process by modulating the EGFR pathway in spermatocytes (Chen et al., 2016b), we examined whether the expression of the EGFR is affected in the hnRNPH1 cKO spermatocytes. Both IF and western blot results showed that the p-EGFR level is significantly increased in hnRNPH1 cKO testes while the total EGFR expression appears unchanged (Fig. S6D-G). qPCR was then performed to check whether hnRNPH1 ablation in SCs has similar effects on the mRNA expression of meiosis-related genes as AR deletion in SCs. As shown in Fig. S7A, some of the tested genes, including the *Rad51* and *Dmc1*, are downregulated in hnRNPH1 cKO testes. Furthermore, compared with controls, the protein levels of RAD51 and DMC1, and their localization on chromosomes in the hnRNPH1 cKO spermatocytes were significantly decreased (Fig. S7B-I), which is consistent with AR cKO mice (Chen et al., 2016b). These results suggest that hnRNPH1 in SCs may regulate the gene transcription of meiosis by cooperation with AR. To further understand the underlying molecular regulation of hnRNPH1 in gene transcription, the previous ChIP-seq data (Xiao et al., 2019) of hnRNPH1 in HepG2 cells were re-analyzed to clarify whether hnRNPH1 has

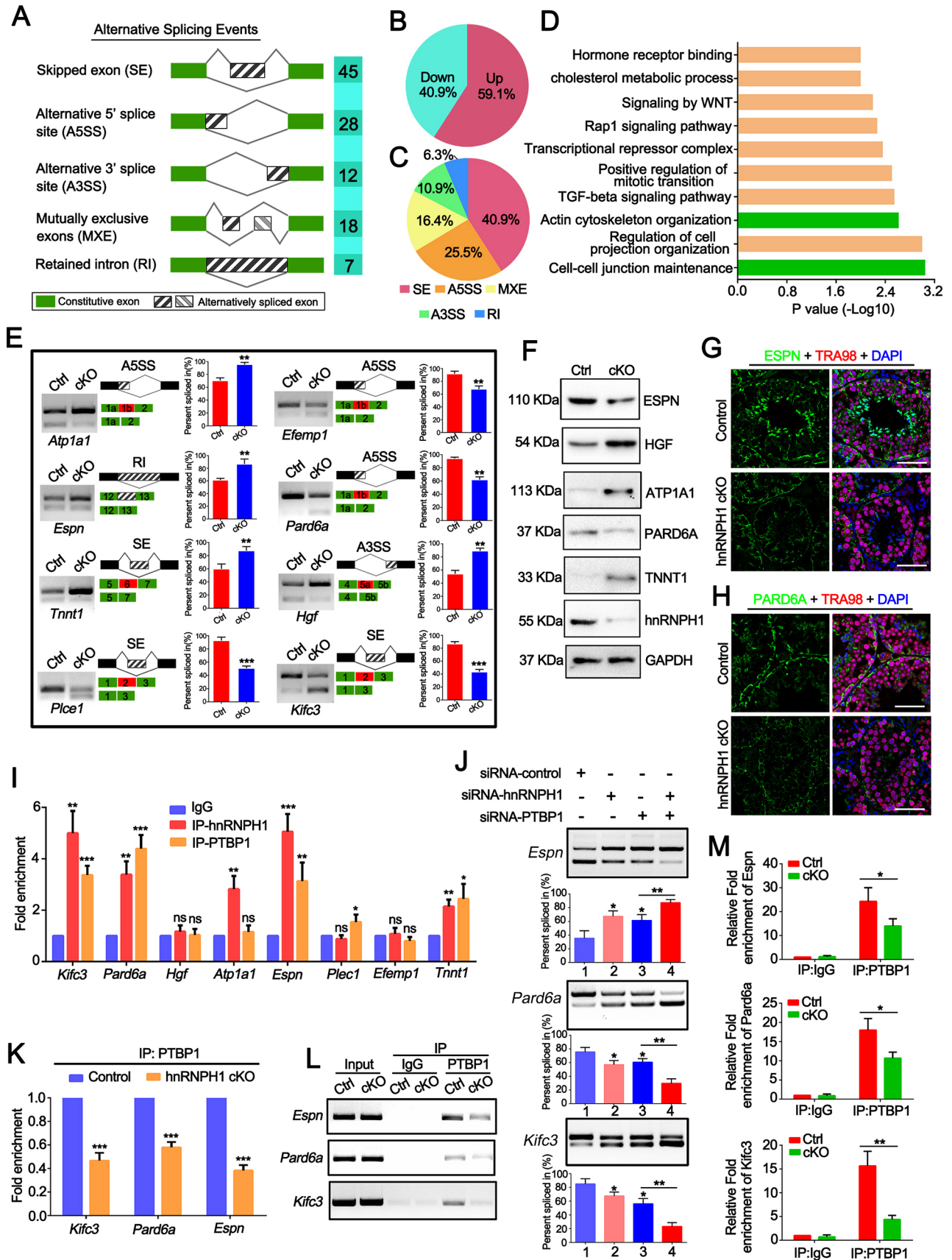


Fig. 5. See next page for legend.

Fig. 5. hnRNPH1 and PTBP1 co-regulated the alternative splicing of cell junction-related genes in SCs. (A) Different types of alternative splicing (AS) identified in hnRNPH1 cKO SCs are shown. Numbers on the right are the amount of corresponding misregulated splicing events in hnRNPH1 cKO SCs. (B) Pie chart showing percentages of changed AS events identified in hnRNPH1 cKO SCs versus control SCs. (C) Pie chart representing the distribution of regulated splicing events among different splicing patterns in hnRNPH1 cKO SCs versus control SCs. (D) GO-term enrichment analyses of AS changed genes caused by hnRNPH1 deficiency in SCs. (E) Representative examples of RT-PCR analyses for indicated AS events for genes differentially regulated in control and hnRNPH1 cKO SCs. Middle panels are schematic diagrams of alternatively spliced exons detected by RNA-seq analysis. Right panels show the quantification of percentage spliced in index (PSI). Data are mean±s.d., $n=3$. ** $P\leq 0.01$, *** $P\leq 0.001$ (unpaired Student's *t*-test). (F) Western blot analyses of the expression of ESPN, HGF, ATP1A1, PARD6A, TNNT1 and hnRNPH1 in control and hnRNPH1 cKO SCs. GAPDH was used as a loading control. (G,H) Co-immunofluorescence staining of TRA98 with ESPN (G) and with PARD6A (H) on testis sections from control and hnRNPH1 cKO mice at P56. Scale bars: 50 μm . (I) Histograms show RIP-qPCR analyses of selected mRNA of eight genes co-precipitated using anti-hnRNPH1, anti-PTBP1 antibodies and control IgG in RIP experiments performed from purified SCs. (J) RT-PCR analyses of splicing assays were performed in HEK293T cells transfected with the indicated minigenes and knockdown-related vectors for hnRNPH1 and PTBP1. The corresponding quantification of percent spliced in index (PSI) are also shown. Data are mean±s.d., $n=3$. * $P\leq 0.05$, ** $P\leq 0.01$ (one-way ANOVA). (K,L) RIP-qPCR (K) and RT-PCR (L) analyses of the association of the selected gene mRNAs with PTBP1 in control and hnRNPH1 cKO SCs are shown. Data are mean±s.d., $n=3$. *** $P\leq 0.001$ (unpaired Student's *t*-test). (M) Quantification of relative fold enrichment of indicated genes in L. Data are mean±s.d. * $P\leq 0.05$, ** $P\leq 0.01$ (unpaired Student's *t*-test).

the ability to bind DNA. The result showed a large number of binding peaks of hnRNPH1 near the promoter and the transcription start site (TSS) of more than 10,000 genes (Table S4), suggesting that hnRNPH1 could bind to the promoter of many genes. Combined with our RNA-seq data, a total of 143 differentially expressed genes (105 upregulated and 38 downregulated) were found to overlap with the genes whose promoters are bound by hnRNPH1 (Fig. S7J), suggesting that hnRNPH1 may directly bind to the promoters of these genes to regulate their transcription.

As mentioned above, hnRNPH1 can interact with AR, a transcription factor highly expressed in SCs; we thus speculated that hnRNPH1 might participate in transcriptional regulation as a co-factor of AR. Combined with the previous ChIP-seq data of AR (Raut et al., 2021), a total of 50 differentially expressed genes (35 upregulated and 15 downregulated) were found to be bound by hnRNPH1 and AR (Fig. 6I). GO term analysis indicated that these genes are mainly involved in 'cell-cell adhesion' and 'extracellular matrix organization' (Fig. 6J). Thereafter, 10 out of these genes were selected for ChIP-qPCR verification and it was found that six of the tested genes (*Smoc2*, *Vwa1*, *Lrp2*, *Itga6*, *Pkp2* and *Nfasc*) have their promoter bound by hnRNPH1 and AR (Fig. 6K). To further explore whether hnRNPH1 can regulate the gene transcription by cooperation with AR, two target genes (*Pkp2* and *Itga6*) were selected for the luciferase reporter assay because of their known role in modulating BTB structure. Luciferase reporter plasmids containing the promoters (2 kb fragment upstream of the TSS of *Pkp2* and *Itga6*) were transfected into HEK293T cells with other vectors. After treatment with DHT (an activator of AR), exogenous AR translocated to the nucleus in HEK293T cells (Fig. S7K), and the *Pkp2* and *Itga6* reporter activities were slightly increased compared with control cells (Fig. 6L). When AR and hnRNPH1 are overexpressed together, both reporter activities were significantly higher than when overexpressing only AR (Fig. 6L),

and both AR and hnRNPH1 were completely colocalized in the nucleus under DHT stimulation (Fig. S7K). Interestingly, if we transfected only *Hnrnp1* in the absence of AR or transfected *Hnrnp1* with AR but without DHT, the transcriptional activity of the target gene did not change or only increased slightly (Fig. 6L). Additionally, the ability of AR to bind the two target genes is severely affected by hnRNPH1 deletion (Fig. S7L). These data suggest that hnRNPH1 can promote the transcription of some target genes by modulating the AR activity, and AR activity is required for *Hnrnp1* transcriptional activation.

DISCUSSION

The functions of SCs in spermatogenesis have attracted considerable attention recently. Although the functions of some genes and signaling pathway in SCs has been elucidated (Ni et al., 2019), the gene regulatory network establishing the crosstalk between SCs and germ cells remain unclear. In the current study, we found that hnRNPH1, a RNA-binding protein, is highly expressed in SCs and interacts with the splicing factor PTBP1 and the transcription factor AR, which have been demonstrated to regulate spermatogenesis in SCs. hnRNPH1 deletion in SCs led to compromised BTB function, delayed meiotic progression, increased germ cell apoptosis, sloughing of germ cells and eventually infertility of mice. Furthermore, we revealed that, in the SCs, hnRNPH1 regulates the mRNA splicing by cooperating with PTBP1; it also works with AR to regulate the gene transcription and, notably, some target genes regulated by both AR and hnRNPH1 are known to be involved in the establishment of crosstalk between SCs and germ cells. Interestingly, our recently published study elucidated the role of hnRNPH1 in germ cells and found that it can cooperate with the critical splicing factors PTBP2 and SRSF3 to regulate the alternative splicing of their target genes that are involved in the normal development of spermatogenic cells (Feng et al., 2022). Although hnRNPH1 plays a similar role in germ cells and SCs to support spermatogenesis by modulating mRNA splicing, its interacting proteins, regulated target genes and signal pathways are distinct in each cell type. Thus, combined with our published study, the current study added another layer of the function of hnRNPH1 on spermatogenesis, highlighting the vital roles of hnRNPH1 in establishing the crosstalk between SCs and germ cells during spermatogenesis; however, this study also hints at a complex gene regulatory network in testes.

One of the crucial findings in this study is that hnRNPH1 ablation in SCs resulted in severe damage to the BTB structure with abnormal microtubule distribution and disordered cytoskeleton, which compromises SC functions (Fig. 4B-D). The BTB is a specialized cell junction between adjacent SCs that prevents the deleterious exchange of macromolecules between blood and seminiferous tubules (Stanton, 2016). Adhesion, gap and occluding junctions constitute the basis of the BTB, which are interspersed with tubulobulbar complexes and actin-based cytoskeletal structures (Dunleavy et al., 2019). Our RNA-seq data revealed that, among the splicing changed and differentially expressed genes, many are identified to be involved in the cell junctions, which supports the phenotype of the BTB structure disruption. Another important readout of SC function and structure is the disruption of apical ES, which may be a cause of spermatids sloughing into the young adult epididymis, much like our recent report that depletion of the *Uhrfl* gene in SCs disrupts the intact structure of the BTB and ES, leading to spermatids sloughed from seminiferous tubule (Wu et al., 2022). However, the role of other genes related to cell adhesion and cytoskeletal structures in SCs has

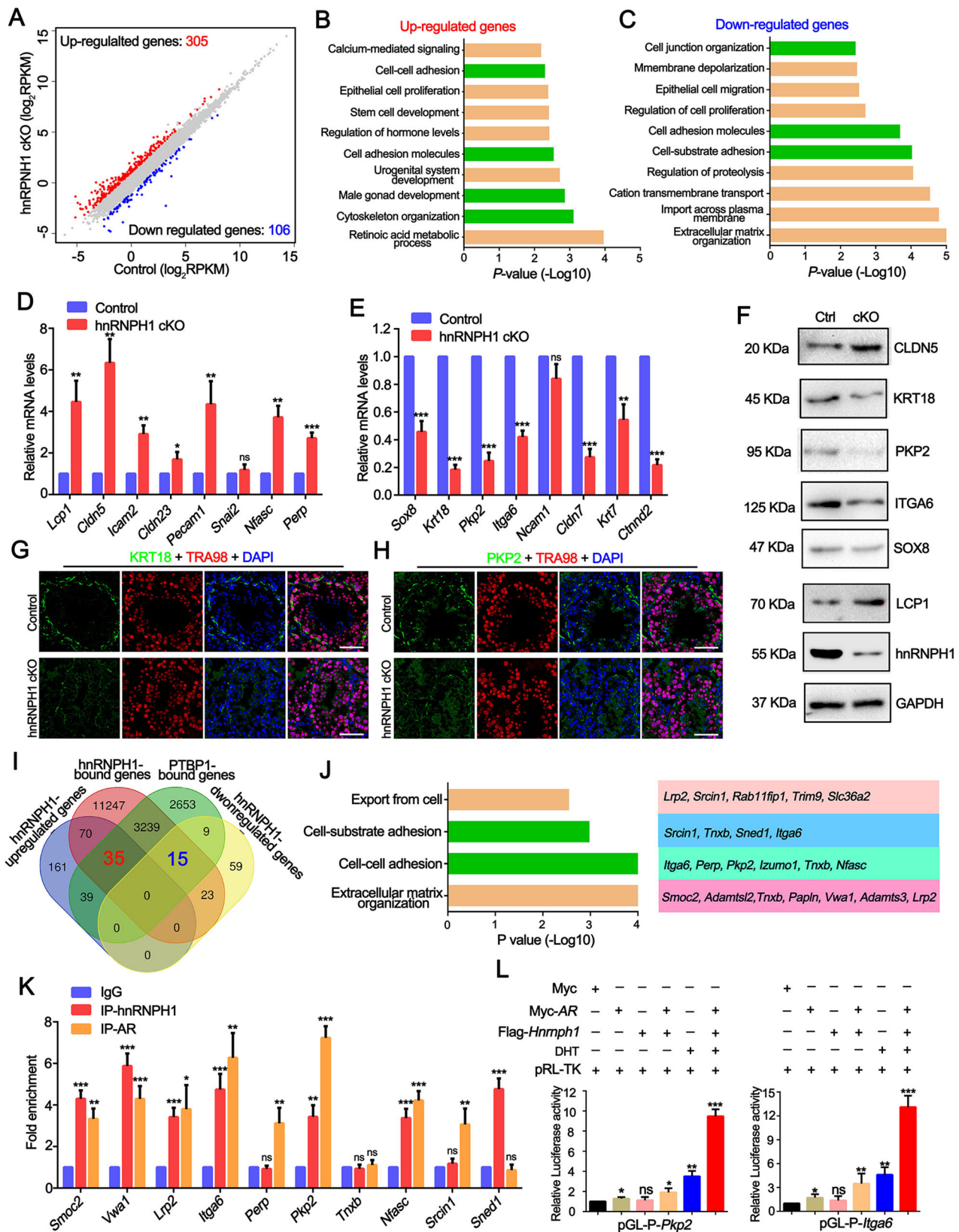


Fig. 6. See next page for legend.

not been studied; these may also contribute to BTB damage and need to be further investigated. In addition, the SCs of hnRNPH1 cKO mice showed abnormal morphology with short pseudopodia

unable to extend into the lumen of the seminiferous tubule, thus likely affecting its junction with germ cells (especially post-meiotic germ cells). This may be why some round spermatids sloughed from

Fig. 6. hnRNPH1 cooperates with AR to regulate the transcription of the cell junction-related genes in SCs. (A) Scatter plots showing the differentially expressed genes in hnRNPH1 cKO SCs. (B,C) GO term analyses of the 305 upregulated genes (B) and 106 downregulated genes (C) in hnRNPH1 cKO SCs are shown. The 10 enriched GO pathways in the upregulated and downregulated genes are illustrated by gene counts and *P*-values. (D,E) RT-qPCR validates the selected upregulated (D) and downregulated (E) genes that are associated with the cell junction in hnRNPH1 cKO SCs from RNA-seq data. Data are mean±s.e.m., *n*=3. **P*≤0.05, ***P*≤0.01, ****P*≤0.001 (unpaired Student's *t*-test). (F) Western blot analyses of the expression of CLDN5, KRT18, PKP2, ITGA6, SOX8, LCP1 and hnRNPH1 in control and hnRNPH1 cKO SCs isolated from P21 mice. GAPDH was used as a loading control. (G,H) Co-immunofluorescence staining of TRA98 with KRT18 (G) and PKP2 (H) in adult control and hnRNPH1 cKO testes, respectively. Scale bars: 50 μm. (I) Venn diagrams showing overlap of hnRNPH1-regulated differentially expressed genes, hnRNPH1-bound genes and PTBP1-bound genes in SCs. (J) GO term enrichment analyses of hnRNPH1-regulated differentially expression genes bound by both hnRNPH1 and PTBP1 in SCs. (K) Histograms show ChIP-qPCR analyses of the mRNA of 10 selected genes precipitated by anti-hnRNPH1, anti-AR antibodies and control IgG in ChIP experiments performed in SCs. Data are mean±s.e.m., *n*=3. **P*≤0.05, ***P*≤0.01, ****P*≤0.001 (unpaired Student's *t*-test). (L) Luciferase-based reporter assays show the luciferase activity of the *Pkp2* (left) and *Itga6* (right) promoter region in SCs significantly increases when hnRNPH1 is overexpressed. Data are mean±s.e.m., *n*=3. **P*≤0.05, ***P*≤0.01, ****P*≤0.001 (unpaired Student's *t*-test).

the seminiferous tubules and prematurely entered the lumen of the epididymis. Of note, in addition to the cell junction-related genes, many genes that belong to other categories, such as 'cation transmembrane transport' (de Liz Oliveira Cavalli et al., 2013), 'TGF-beta signaling pathway' (Sun et al., 2008), 'Rap1 signaling pathway' (Berruti and Paiardi, 2014), 'Signaling by WNT' (Tanwar et al., 2010) and 'cholesterol metabolic process' (Shi et al., 2018) were also closely related to the SCs development (Fig. 5D). Thus, we cannot rule out the possibility that hnRNPH1 ablation in SCs could affect many aspects of SC function.

SCs exhibit extraordinary stage specificity in mRNA and protein expression because they must adapt to the changing needs of the germ cells (Johnston et al., 2008). As a RNA-binding protein, hnRNPH1 showed high protein expression in the SCs from P14 onwards (Fig. 1C), which likely started to function from the meiotic stage because the phenotypic defects of hnRNPH1 cKO mice began to appear during the meiotic stage. Otherwise, although the spermatocytes showed developmental retardation and even underwent apoptosis, many of them could enter the post-meiotic stage. We speculate that the following reasons may explain this phenotype: first, a small amount of residual hnRNPH1 protein exists in some SCs due to low knockout efficiency (although it cannot be observed by IF whether these SCs can still support adjacent spermatocytes to develop normally); second, the SCs are heterogeneous, and in some of these cells loss of hnRNPH1 has been compensated for by other unknown homologous proteins; third, spermatocytes may show different degrees of connection with SCs depending on their spatial distribution, leading to those spermatocytes that are not closely connected with SCs being more prone to apoptosis and/or developmentally delayed due to the lack of support from SCs. Considering the significantly decreased number of post-meiotic germ cells (especially the elongating spermatids), this raises a possible role for hnRNPH1 in SCs in the balance of gene expression to maintain the normal function of SCs during multiple spermatogenesis stages.

Previous studies mainly focused on the role of hnRNPH1 in the control of alternative splicing (Uren et al., 2016), and herein we also

found some splicing factors were the potential interacting partner of hnRNPH1 in the SCs, such as PTBP1, NONO and SFPQ. In this study, hnRNPH1 has been found to cooperate with PTBP1 to regulate the mRNA splicing of TCF3, a transcription factor that plays an essential role in stem cell maintenance (Yamazaki et al., 2019). PTBP1 was reported to be present in SCs and to regulate the BTB structure (Yang et al., 2021), but the relevant mechanisms are unclear. This study demonstrates their coordinated regulation in supporting SC function, suggesting that they may participate in the various biological processes as cooperators. Moreover, this finding reveals that hnRNPH1 and PTBP1 can bind some target genes and cooperate to regulate their mRNA splicing in SCs. More interestingly, the binding affinity of PTBP1 to some target genes (*Espn* and *Pard6a*) in SCs was significantly decreased in the absence of hnRNPH1, indicating that hnRNPH1 could recruit the PTBP1 to its target genes to regulate the alternative splicing. However, PTBP1 was not recruited to all the hnRNPH1 target genes, indicating a selective association between hnRNPH1 and PTBP1 (or other splicing factors) by specific target genes. Of note, alternative splicing could typically generate protein isoforms with different biological properties that differ in their protein interactions, subcellular localization or catalytic ability, or could introduce premature stop codons in their mRNAs, resulting either in the formation of truncated proteins or in the degradation of the mRNA by nonsense-mediated decay (Chen and Manley, 2009). In the current study, based on the RNA-seq data, we found that the mRNA level of these genes with abnormal splicing in hnRNPH1 cKO SCs was almost unchanged, suggesting that the abnormal splicing did not affect the mRNA expression or stability of these genes upon hnRNPH1 depletion in SCs. Moreover, no protein isoforms were observed in our western blot results (Figs 5F and 6F), but the expression levels of these target proteins changed. In fact, alternative splicing can also generate mRNAs that differ in their untranslated regions (UTRs) or coding sequence, and these differences might affect mRNA localization or translation, in addition to mRNA stability (Baralle and Giudice, 2017). Therefore, many alternative splicing events are unnecessary for producing functional proteins. This can be explained in several ways: first, the abnormal transcripts could be non-coding and thus not translated into a protein; second, abnormal mRNA localization could prevent the correct function of the transcript; and third, the efficiency of mRNA translation could be seriously affected. Our data indicate that the abnormal splicing of these genes results in altered protein expression levels but not in the production of other protein isoforms; however, the detailed mechanism needs to be further investigated.

In this study, another exciting previously unreported finding is that hnRNPH1 can interact with the AR to regulate gene transcription in SCs by binding gene promoters. In fact, many RNA-binding proteins are able to bind to DNA to participate in transcriptional regulation (Xiao et al., 2019), such as HNRNPK (Pintacuda et al., 2017), HNRNPL (Kuninger et al., 2002) and hnRNPU (Wen et al., 2021). Indeed, we found that hnRNPH1 can bind to a vast number of gene promoters by re-analyzing previously published ChIP data (Xiao et al., 2019). hnRNPH1 has not been reported to function as a transcription factor, but we speculate that it is more likely that a recruiter of transcription factors regulates the transcription of its target genes as the transcription level of the target genes is significantly increased only in the presence of hnRNPH1 despite activated AR (Fig. 6L). Interestingly, hnRNPH1 has previously been found to interact with AR to control prostate tumorigenesis *in vivo*, to promote the expression of AR and to prime the activation of androgen-regulated genes (Yang et al., 2016).

However, this finding revealed that hnRNPH1 did not affect AR expression in SCs, but promoted the transcription of target genes by interacting with AR, suggesting the complex of hnRNPH1 and AR may play different roles in diverse contexts. In addition, in the present study, we found that hnRNPH1 deletion may affect AR recruitment to promoters of some of its target genes in SCs (Fig. S7L). Combining our luciferase assay data (Fig. 3L), it is highly likely that hnRNPH1 regulates the transcriptional activity of AR as a co-factor in SCs and recruits AR to the promoters of target genes through its RRM domain to promote their transcription but not the RNA-mediated processes. As one of the SC markers, AR regulates the meiotic process by modulating the EGFR pathway, which affects the expression of the meiosis-related genes in germ cells (Chen et al., 2016b). Interestingly, in the current study, some genes associated with the EGFR pathway could also be regulated by hnRNPH1, and meiosis-related genes (such as *Rad51* and *Dmc1*) were affected in the hnRNPH1 cKO germ cells. However, AR ablation in mice resulting in meiosis defects was much more severe than hnRNPH1 depletion in mouse SCs. This suggests that the functions of hnRNPH1 and AR in SCs in regulating meiotic processes are only partially overlapped. Of note, hnRNPH1 has also been reported to play roles in other biological processes, such as mRNA decay and translation (Uren et al., 2016); in the current study, the protein levels of many DEGs were found to be changed in hnRNPH1-deficient SCs (Fig. 6F-H). Meanwhile, many proteins associated with RNA degradation were identified from our IP-MS data (Fig. 3B). Therefore, the possible functions of hnRNPH1 in the post-transcriptional regulation of SCs cannot be excluded and needs to be investigated further.

In summary, this study uncovers an essential role for hnRNPH1 in SCs in maintaining the BTB integrity and supporting normal meiosis. It also expands our understanding of the physiological functions of SCs in regulating spermatogenesis. These findings reveal a previously unreported mechanism by which hnRNPH1 regulates the alternative splicing by recruiting the splicing factor PTBP1 and controls the gene transcription through cooperation with the transcription factor AR (Fig. S8). This provides new insights into the gene regulatory network of hnRNPH1 in SCs that regulate the expression of target genes that are essential for establishing crosstalk between SCs and germ cells.

MATERIALS AND METHODS

Mice

All animal work was performed and approved by the Institutional Animal Care and Use Committee (IACUC) of Huazhong University of Science and Technology. Floxed hnRNPH1 mice (*Hnrnp1^{lox/lox}*) were generated by embryonic cell (ESC) targeting and blastocyst injection at the Model Animal Research Center of Nanjing (T001430). In brief, ESCs were targeted by carrying two loxP sites flanked in exon 6 and a neomycin selection cassette flanked by FRT sites in introns 5 and 6 of *Hnrnp1*. The *Hnrnp1^{+/+}* mice were obtained by chimera formation and germline transmission. Mice were then crossed with FLP transgenic mice to remove the neomycin cassette and maintained on a C57BL/6J background. The Amh-Cre mouse strain in the C57BL/6J background was purchased from the Jackson Laboratory. Amh-Cre recombinase had recombinase activities in SCs (Lécureuil et al., 2002). Amh-Cre males were first crossed with *Hnrnp1^{lox/lox}* females to generate the Amh-Cre; *Hnrnp1^{+/lox}* males, then the Amh-Cre; *Hnrnp1^{+/lox}* male mice were bred with *Hnrnp1^{lox/lox}* female mice to obtain the Amh-Cre; *Hnrnp1^{lox/Δ}* (designated as hnRNPH1 cKO) males. The primers for genotyping are listed in Table S5.

Fertility test

Sexually mature (older than 8 weeks) control and hnRNPH1 cKO male mice were caged with fertility-proven female mice for 5 months, respectively.

The females were checked for vaginal plugs every morning. The plugged females were separated and single caged, and the pregnancy was recorded. The number of pups in each cage was also recorded after birth.

Western blotting

The indicated samples were collected and lysed in ice-cold RIPA buffer (CW BIO, 01408). Protein extracts were rotated at 4°C for 10 min and centrifuged at 12,000 *g* for 15 min at 4°C. They were then denatured with 5× SDS loading buffer (Beyotime, P0015L) at 100°C for 10 min. The prepared proteins were separated by SDS-PAGE on 10% resolving gels and transferred to a PVDF membrane (Bio-Rad). The membrane was probed with primary and secondary antibodies (Table S6). Images were detected with ECL according to the manufacturer's instructions (Clarity Western ECL Substrate, Bio-Rad).

Immunoprecipitation

Mouse tissues or cells were homogenized in ice-cold RIPA buffer (CW BIO, 01408) and the resultant cell extracts were treated with or without a mix of RNaseA and DNase (1 μg/ml) at 4°C for 1 h, followed by clarification of the lysates by centrifugation at 13,000 *g* for 25 min. The relevant antibodies and pre-cleaned magnetic protein A/G beads were then incubated with the tissue lysates overnight at 4°C. The beads were washed with Cell lysis buffer for Western and IP (Beyotime, P0013) with protease inhibitor cocktail (P1010, Beyotime) and then boiled in 5× SDS loading buffer (Beyotime, P0015L) for western blotting analyses.

Glutathione S-transferase (GST) pull-down assay

The recombinant plasmids pGEX4G-1-glutathione S-transferase (GST)-hnRNPH1 and GST empty vectors were transformed into *Escherichia coli* DH5α cells, and expression was induced using isopropyl thiogalactoside (IPTG) at 20°C for 8 h. The cells were then harvested and lysed using ultrasound, and centrifuged to separate the supernatant. The soluble cell lysates containing GST or GST-hnRNPH1 were incubated with GST beads at 4°C for 6 h and then washed with PBS buffer. Then the GST beads were collected and incubated with isolated mouse SC lysates overnight at 4°C followed by washing as described above. Finally, the sodium dodecyl sulfate-polyacrylamide gel (SDS-PAGE) electrophoresis was used to detect the binding of AR and PTBP1.

Transmission electron microscopy (TEM)

TEM of mouse testis followed a previously described protocol (Wang et al., 2018). Briefly, the adult testes were collected from control and hnRNPH1 cKO mice then fixed in 0.1 M cacodylate buffer (pH=7.4) containing 3% paraformaldehyde and 3% glutaraldehyde plus 0.2% picric acid for 2 h at 4°C and for 1 h at room temperature. After washing with 0.1 M cacodylate buffer, the samples were post-fixed with 1% OsO₄ for 1 h at room temperature. The samples were then dehydrated in sequential ethanol solutions (30, 50, 70, 90 and 100%) and embedded in an Eponate mixture (Electron Microscopy Sciences) for polymerization for ~24 h at 60°C. Ultrathin sections (~70 nm) were cut with a diamond knife. After staining with uranyl acetate and lead citrate, the sections were photographed using a transmission electron microscope (Tecnai G2 12, FEI).

Histological analyses and immunohistochemistry

Testes from control and hnRNPH1 cKO mice were fixed in Bouin's solution (Sigma-Aldrich, HT10132) overnight at 4°C and then dehydrated in graded ethanol (50, 70, 95 and 100%). 5 μm sections were cut after they were embedded in paraffin wax. Periodic acid-Schiff (PAS) staining was performed using a standard protocol. For the immunohistochemistry, 5 μm tissue sections were prepared with embedded mouse testes in paraffin wax. After dewaxing and hydration, they were microwaved for antigen retrieval by 0.01% Tris-EDTA (pH 9.0). The tissues were then washed three times using PBS and treated with 3% H₂O₂ at room temperature for 15 min. After washing with PBS thoroughly, the sections were blocked in 5% BSA for 1.5 h at room temperature and then incubated with primary antibodies at 4°C overnight. The sections were then incubated with a secondary antibody for 1.5 h at room temperature. After coloring with DAB at room

temperature, the sections were stained with Hematoxylin and washed with double-distilled H₂O. The sections were then mounted using neutral resin and photographed after hydration.

Immunofluorescence and TUNEL staining

For immunofluorescence, testes were fixed in 4% paraformaldehyde overnight at 4°C, dehydrated in 20% sucrose and embedded in Tissue-Tek optimal cutting temperature (OCT). Frozen sections (5 µm) were cut, followed by antigen retrieval with 0.01 M sodium citrate buffer (pH 6.0). After blocking for 1 h, the sections were incubated with primary and secondary antibodies (Table S6). TUNEL staining was performed on frozen sections using the In Situ Cell Death Detection kit, Fluorescein (Roche), according to the manufacturer's instructions. The images were captured using a Scope A1 microscope (Zeiss) with a digital camera (MSX2, Micro-shot Technology).

Biotin tracer

The control and hnRNPH1 cKO mice were anesthetized, and then the testes were sequentially exteriorized and injected with biotin tracer dye (Thermo Fisher Scientific). Mice were kept anesthetized for 30 min and euthanized. Testes were harvested, fixed in 4% formaldehyde and sectioned at 5 µm. Sections were blocked with 10% normal goat serum followed by incubation with FITC-conjugated streptavidin (Invitrogen) and DAPI.

Meiotic chromosome spread analyses

Chromosome spreads were prepared as previously reported with slight modifications (Alavattam et al., 2018). In brief, testes were collected from euthanized mice and the tunica albuginea was removed. Testicular seminiferous tubules were pretreated by hypotonic buffer [30 mM Tris, 50 mM sucrose, 17 mM trisodium citrate dihydrate, 5 mM EDTA, 0.5 mM DTT and 0.5 mM phenylmethylsulfonyl fluoride (PMSF) (pH 8.2)] for 1 h. The seminiferous tubules were mashed with tweezers and were suspended in 100 mM sucrose for dispersing into single cells and spreading as a thin cell layer on slides, which were soaked in 2% (w/v) paraformaldehyde solution treated with 0.15% Triton X-100. The prepared slides were placed in closed humid chambers for 4 h at room temperature. After incubation, the damp slides were washed with 0.4% Photo-Flo (Kodak, 1464510), followed by air-drying at room temperature for 30 min, and then stored at -80°C for later immunostaining.

Primary SC cultures

Primary cultures of SCs were performed as described previously (Wu et al., 2022), with slight modifications. Briefly, testes from mice at P21 were decapsulated and digested with collagenase IV (1 mg/ml) at 37°C for 10 min. The supernatant containing Leydig/interstitial cells was removed after the seminiferous tubules were allowed to settle down. Seminiferous tubules were then treated with trypsin (2.5 mg/ml) and DNase I (0.5 mg/ml) for 15 min at 37°C in the shaker. After being treated with trypsin inhibitor, the mixed cells containing SCs were centrifuged (300 g/min), washed (three times with DMEM/F12 medium) and filtered (40 µm pore-size nylon mesh) to prepare a single-cell suspension, and then cultured in dishes at 35°C in the DMEM/F12 medium containing 10% FBS. After a 48 h culture, the cells were treated with hypotonic solution [20 mM Tris-HCl (pH 7.4)] for 3 min, followed by washing with DMEM/F12 three times to remove residual germ cells and other types of cells. Pure SCs were cultured for 24 h and then resuspended on Matrigel (Corning)-coated culture dishes or microscopic cover glasses, depending on their use in subsequent experiments. First, 60 mm culture dishes at 0.5×10^6 cells/cm² containing 5 ml DMEM/F12 or six-well culture dishes at 0.5×10^6 cells/cm² containing 3 ml DMEM/F12 were used for lysate preparation or RNA extraction. Second, microscopic (10 mm round) cover glasses at 0.05×10^6 cells/cm² were placed in 12-well dishes containing 2 ml DMEM/F12 per well for dual-labeled immunofluorescence analysis. The immunofluorescence staining of WT1 and TRA98 determined the purity of the isolated primary SCs and was more than 90% (Fig. 1B).

RNA isolation, RT-PCR and RT-qPCR

Total RNA was extracted from the samples by using Trizol reagent (Thermo Fisher Scientific). The concentration and purity of RNA were determined by absorbance at 260/280 nm. Total RNA (1 µg) was reverse transcribed using a HiScript II 1st Strand cDNA Synthesis Kit (Vazyme Biotech) according to the manufacturer's instructions. RT-PCR primers designed to amplify two or multiple isoforms of different sizes are shown in Table S5. PCR products were quantified using Image J software. Splicing ratios are represented as PSI (percent spliced in) values, representing the percentage of mRNA transcripts of a gene that include a specific exon or splice site. We quantitated the relative expression of genes of interest by real-time qPCR (RT-qPCR) using the SYBR green master mix, (TaKaRa) according to the manufacturer's instructions.

Plasmid and minigene construction

Full-length and indicated fragments of *Hnrnp1* cDNA were cloned into a pCMV vector containing the N-terminal Flag epitope tag, and full-length and indicated fragments of AR and *Ptbp1* cDNAs were cloned into a pCMV vector containing the N-terminal c-Myc epitope tag. HEK293T cells were transfected with indicated plasmids using Lipofectamine 2000 (Life Technologies). After 36 h, immunoprecipitation was performed using anti-Flag rabbit polyclonal antibody (5 µg antibody in 500 µl cell lysate, 20543-1-AP, Proteintech), followed by a western blot to identify protein interactions. For minigenes construction, the *Espn*, *Pard6a*, *Kifc3* and *Tnnt1* minigenes were amplified from genomic DNA of adult mouse testis using primers shown in Table S5, and then the minigenes were cloned into pCDNA3.1(-) vector and validated by sequencing.

Luciferase reporter assays

HEK293 cells were transfected with luciferase reporter plasmids (120 ng) linked with the *Pkp2* and *Iga6* promoters using Lipofectamine LTX transfection reagent when cells were ~80% confluent. The media were changed after 4-6 h for media with vehicle (ethanol) or DHT (10^{-8} M). The cells were then harvested and lysed 24 h later. Luciferase activity was measured using a dual-luciferase reporter assay system following the manufacturer's instructions (Promega).

RIP assays

SCs were purified from control and hnRNPH1 cKO mouse testes at P21, and then lysed in buffer containing 100 mM KCl, 10 mM HEPES (pH 7.0), 0.5% Triton X-100, 5 mM MgCl₂, 1 mM DTT, 0.5% NP-40, RNase inhibitor (100 U/ml) (Invitrogen) and EDTA-free proteinase inhibitor (Roche). A brief sonication using a Bioruptor 200 (Diagenode) was necessary to make the cracking more thorough. The prepared cell lysates were incubated with IgG and anti-hnRNPH1 (or PTBP1)-coupled Protein G overnight at 4°C. After washing the beads with washing buffer [50 mM Tris-HCl (pH 7.4), 0.1% Triton X-100, 500 mM NaCl, 5 mM EDTA, protease inhibitor cocktail and RNase inhibitor], protein-bound mRNAs were extracted with an RNA extraction kit (ZYMO research) and subjected to RT-qPCR assays.

ChIP assays

The purified SCs from control and hnRNPH1 cKO mice at P21 were crosslinked in 1% formaldehyde diluted in PBS for 20 min and then inactivated with 0.125 M glycine for 5 min at room temperature. Then cells were lysed, and the DNA fragments were broken into an average of 150-800 bp using the SimpleChIP Plus Enzymatic Chromatin IP Kit (Magnetic Beads) according to the manufacturer's instructions. Immunoprecipitation was performed with hnRNPH1 and AR antibody, and IgG-coupled beads. Immunoprecipitated and input DNAs were precipitated with ethanol after de-crosslinking and were then analyzed using a real-time qPCR assay.

RNA-seq analyses

Total RNA was isolated from primary cultured SCs (three biological repeats from control and hnRNPH1 cKO mouse testes at P21) using TRIzol reagents (Invitrogen). The RNA concentration was verified using a NanoDrop 2000 Spectrophotometer (Thermo Fisher Scientific). Total RNA (1 µg) was used from each sample to prepare the mRNA libraries using a TruSeq Stranded

mRNA Library Preparation Kit Set A (RS-122-2101, Illumina) according to the manufacturer's instructions. All libraries were sequenced using the Illumina HiSeq 4000 platform. The FASTX-Toolkit was used to remove adaptor sequences and low-quality reads from the sequencing data. To identify all the transcripts, we used Tophat2 and Cufflinks to assemble the sequencing reads based on the UCSC MM10 mouse genome. The differential expression analysis was performed by Cuffdiff. The differential expressed genes were set with the threshold of $P < 0.05$ and fold change ≥ 2 .

Statistical analyses

All data are mean \pm s.e.m. unless otherwise noted in the figure legends. Statistical differences between datasets were assessed using one-way ANOVA or a unpaired Student's *t*-test using the SPSS16.0 software ($*P < 0.05$, $**P < 0.01$, $***P < 0.001$ and $****P < 0.0001$).

Acknowledgements

We are grateful for engaging in discussions with colleagues and Yuan lab members from Huazhong University of Science and Technology, China, in the very initial phase of the project.

Competing interests

The authors declare no competing or financial interests.

Author contributions

Conceptualization: S.F., X.W., S.Y.; Methodology: S.F., H.W., K.L., M.X., J.L., C.L., J.Z., X.M.; Software: S.F., Y.G.; Validation: S.F., C.L.; Formal analysis: S.F., M.X., J.L., Y.G.; Investigation: S.F., H.W., K.L., M.X., J.L., C.L., J.Z.; Resources: S.F.; Data curation: S.F., H.W., K.L., J.L., Y.G.; Writing - original draft: S.F.; Writing - review & editing: S.Y.; Supervision: X.W., S.Y.; Project administration: S.Y.; Funding acquisition: S.Y.

Funding

This work was, in part, supported by grants from the National Natural Science Foundation of China (82171605 to S.Y. and 31900606 to S.F.); the Strategic Collaborative Research Program of the Ferring Research Institute of Reproductive Medicine, Ferring Pharmaceuticals and the Chinese Academy of Sciences (FIRMSC200502 COV02 to S.Y.); and the Science Technology and Innovation Commission of Shenzhen Municipality (JCYJ20170818160910316 to S.Y.).

Data availability

All RNA-seq and RIP-seq data have been deposited in the NCBI SRA database under accession number PRJNA847021.

Peer review history

The peer review history is available online at <https://journals.biologists.com/dev/article-lookup/doi/10.1242/dev.201040>

References

- Alavattam, K. G., Abe, H., Sakashita, A. and Namekawa, S. H. (2018). Chromosome spread analyses of meiotic sex chromosome inactivation. *Methods Mol. Biol.* **1861**, 113-129. doi:10.1007/978-1-4939-8766-5_10
- Baralle, F. E. and Giudice, J. (2017). Alternative splicing as a regulator of development and tissue identity. *Nat. Rev. Mol. Cell Biol.* **18**, 437-451. doi:10.1038/nrm.2017.27
- Bataclan, M., Leoni, C. and Monticelli, S. (2021). RNA-binding proteins and RNA methylation in myeloid cells. *Immunol. Rev.* **304**, 51-61. doi:10.1111/immr.13025
- Berruti, G. and Paiardi, C. (2014). The dynamic of the apical ectoplasmic specialization between spermatids and Sertoli cells: the case of the small GTPase Rap1. *BioMed Res. Int.* **2014**, 635979. doi:10.1155/2014/635979
- Bressler, R. S. (1976). Dependence of Sertoli cell maturation on the pituitary gland in the mouse. *Am. J. Anat.* **147**, 447-455. doi:10.1002/aja.1001470405
- Catizone, A., Ricci, G. and Galdieri, M. (2008). Hepatocyte growth factor modulates Sertoli-Sertoli tight junction dynamics. *J. Cell. Physiol.* **216**, 253-260. doi:10.1002/jcp.21400
- Chen, M. and Manley, J. L. (2009). Mechanisms of alternative splicing regulation: insights from molecular and genomics approaches. *Nat. Rev. Mol. Cell Biol.* **10**, 741-754. doi:10.1038/nrm2777
- Chen, B., Li, A., Wang, D., Wang, M., Zheng, L. and Bartles, J. R. (1999). Espin contains an additional actin-binding site in its N terminus and is a major actin-binding protein of the Sertoli cell-spermatid ectoplasmic specialization junctional plaque. *Mol. Biol. Cell* **10**, 4327-4339. doi:10.1091/mbc.10.12.4327
- Chen, H., Mruk, D. D., Xia, W., Bonanomi, M., Silvestrini, B. and Cheng, C.-Y. (2016a). Effective delivery of male contraceptives behind the Blood-Testis Barrier (BTB) - lesson from adjuvin. *Curr. Med. Chem.* **23**, 701-713. doi:10.2174/0929867323666160112122724
- Chen, S.-R., Hao, X.-X., Zhang, Y., Deng, S.-L., Wang, Z.-P., Wang, Y.-Q., Wang, X.-X. and Liu, Y.-X. (2016b). Androgen receptor in Sertoli cells regulates DNA double-strand break repair and chromosomal synapsis of spermatocytes partially through intercellular EGF-EGFR signaling. *Oncotarget* **7**, 18722-18735. doi:10.18632/oncotarget.7916
- de Liz Oliveira Cavalli, V. L., Cattani, D., Heinz Rieg, C. E., Pierozan, P., Zanatta, L., Benedetti Parisotto, E., Wilhelm Filho, D., Mena Barreto Silva, F. R., Pessoa-Pureur, R. and Zamoner, A. (2013). Roundup disrupts male reproductive functions by triggering calcium-mediated cell death in rat testis and Sertoli cells. *Free Radic. Biol. Med.* **65**, 335-346. doi:10.1016/j.freeradbiomed.2013.06.043
- Dong, B.-W., Jin, X.-H., Yan, C.-Y., Yang, T., Cai, G.-Q. and Lu, J. (2017). Synergistic upregulation of NONO and PSPC1 regulates Sertoli cell response to MEHP via modulation of ALDH1A1 signaling. *FEBS Lett.* **591**, 914-923. doi:10.1002/1873-3468.12568
- Dunleavy, J. E. M., O'Bryan, M. K., Stanton, P. G. and O'Donnell, L. (2019). The cytoskeleton in spermatogenesis. *Reproduction (Cambridge, England)* **157**, R53-R72. doi:10.1530/REP-18-0457
- Feng, S., Li, J., Wen, H., Liu, K., Gui, Y., Wen, Y., Wang, X. and Yuan, S. (2022). hnRNPH1 recruits PTBP2 and SRSF3 to modulate alternative splicing in germ cells. *Nat. Commun.* **13**, 3588. doi:10.1038/s41467-022-31364-7
- Hasegawa, K. and Saga, Y. (2012). Retinoic acid signaling in Sertoli cells regulates organization of the blood-testis barrier through cyclical changes in gene expression. *Development (Cambridge, England)* **139**, 4347-4355. doi:10.1242/dev.080119
- Jia, X., Xu, Y., Wu, W., Fan, Y., Wang, G., Zhang, T. and Su, W. (2017). Aroclor1254 disrupts the blood-testis barrier by promoting endocytosis and degradation of junction proteins via p38 MAPK pathway. *Cell Death Dis.* **8**, e2823. doi:10.1038/cddis.2017.224
- Johnston, D. S., Wright, W. W., Dicaneloro, P., Wilson, E., Kopf, G. S. and Jelinsky, S. A. (2008). Stage-specific gene expression is a fundamental characteristic of rat spermatogenic cells and Sertoli cells. *Proc. Natl. Acad. Sci. USA* **105**, 8315-8320. doi:10.1073/pnas.0709854105
- Knott, G. J., Bond, C. S. and Fox, A. H. (2016). The DBHS proteins SFPQ, NONO and PSPC1: a multipurpose molecular scaffold. *Nucleic Acids Res.* **44**, 3989-4004. doi:10.1093/nar/gkw271
- Kuninger, D. T., Izumi, T., Papaconstantinou, J. and Mitra, S. (2002). Human AP-endonuclease 1 and hnRNP-L interact with a nCARE-like repressor element in the AP-endonuclease 1 promoter. *Nucleic Acids Res.* **30**, 823-829. doi:10.1093/nar/30.3.823
- Lécureuil, C., Fontaine, I., Crepieux, P. and Guillou, F. (2002). Sertoli and granulosa cell-specific Cre recombinase activity in transgenic mice. *Genesis* **33**, 114-118. doi:10.1002/gene.10100
- Li, M. W. M., Mruk, D. D., Lee, W. M. and Cheng, C. Y. (2009). Connexin 43 and plakophilin-2 as a protein complex that regulates blood-testis barrier dynamics. *Proc. Natl. Acad. Sci. USA* **106**, 10213-10218. doi:10.1073/pnas.0901700106
- Li, J., Guo, W., Li, F., He, J., Yu, Q., Wu, X., Li, J. and Mao, X. (2012). HnRNPL as a key factor in spermatogenesis: Lesson from functional proteomic studies of azoospermia patients with sertoli cell only syndrome. *J. Proteomics* **75**, 2879-2891. doi:10.1016/j.jpro.2011.12.040
- Liu, L. L., Xie, N., Sun, S., Plymate, S., Mostaghel, E. and Dong, X. (2014). Mechanisms of the androgen receptor splicing in prostate cancer cells. *Oncogene* **33**, 3140-3150. doi:10.1038/nc.2013.284
- Lv, C., Larbi, A., Memon, S., Liang, J., Zhao, X., Shao, Q., Wu, G. and Quan, G. (2020). The proteomic characterization of ram sperm during cryopreservation analyzed by the two-dimensional electrophoresis coupled with mass spectrometry. *Cryobiology* **97**, 37-45. doi:10.1016/j.cryobiol.2020.10.011
- Mao, B., Bu, T., Mruk, D., Li, C., Sun, F. and Cheng, C. Y. (2020). Modulating the blood-testis barrier towards increasing drug delivery. *Trends Pharmacol. Sci.* **41**, 690-700. doi:10.1016/j.tips.2020.07.002
- McLachlan, R. I., O'Donnell, L., Meachem, S. J., Stanton, P. G., de Kretser, D. M., Pratis, K. and Robertson, D. M. (2002). Identification of specific sites of hormonal regulation in spermatogenesis in rats, monkeys, and man. *Recent Prog. Horm. Res.* **57**, 149-179. doi:10.1210/rp.57.1.149
- Meng, J., Holdcraft, R. W., Shima, J. E., Griswold, M. D. and Braun, R. E. (2005). Androgens regulate the permeability of the blood-testis barrier. *Proc. Natl. Acad. Sci. USA* **102**, 16696-16700. doi:10.1073/pnas.0506084102
- Morrow, C. M. K., Tyagi, G., Simon, L., Carnes, K., Murphy, K. M., Cooke, P. S., Hofmann, M.-C. C. and Hess, R. A. (2009). Claudin 5 expression in mouse seminiferous epithelium is dependent upon the transcription factor ets variant 5 and contributes to blood-testis barrier function. *Biol. Reprod.* **81**, 871-879. doi:10.1095/biolreprod.109.077040
- Mruk, D. D. and Cheng, C. Y. (2015). The mammalian blood-testis barrier: its biology and regulation. *Endocr. Rev.* **36**, 564-591. doi:10.1210/er.2014-1101
- Neto, F. T. L., Bach, P. V., Najari, B. B., Li, P. S. and Goldstein, M. (2016). Spermatogenesis in humans and its affecting factors. *Semin. Cell Dev. Biol.* **59**, 10-26. doi:10.1016/j.semcd.2016.04.009

- Ni, F.-D., Hao, S.-L. and Yang, W.-X. (2019). Multiple signaling pathways in Sertoli cells: recent findings in spermatogenesis. *Cell Death Dis.* **10**, 541. doi:10.1038/s41419-019-1782-z
- O'Shaughnessy, P. J. (2014). Hormonal control of germ cell development and spermatogenesis. *Semin. Cell Dev. Biol.* **29**, 55-65. doi:10.1016/j.semcdb.2014.02.010
- Pintacuda, G., Wei, G., Roustan, C., Kirmizitas, B. A., Solcan, N., Cerase, A., Castello, A., Mohammed, S., Moindrot, B., Nesterova, T. B. et al. (2017). hnRNPK recruits PCGF3/5-PRC1 to the Xist RNA B-repeat to establish polycomb-mediated chromosomal silencing. *Mol. Cell* **68**, 955-969.e910. doi:10.1016/j.molcel.2017.11.013
- Prudencio, M., Belzil, V. V., Batra, R., Ross, C. A., Gendron, T. F., Pregent, L. J., Murray, M. E., Overstreet, K. K., Piazza-Johnston, A. E., Desaro, P. et al. (2015). Distinct brain transcriptome profiles in C9orf72-associated and sporadic ALS. *Nat. Neurosci.* **18**, 1175-1182. doi:10.1038/nn.4065
- Qu, N., Ogawa, Y., Kuramasu, M., Nagahori, K., Sakabe, K. and Itoh, M. (2020). Immunological microenvironment in the testis. *Reprod. Med. Biol.* **19**, 24-31. doi:10.1002/mb2.12293
- Rajamanickam, G. D., Kastelic, J. P. and Thundathil, J. C. (2017). The ubiquitous isoform of Na/K-ATPase (ATP1A1) regulates junctional proteins, connexin 43 and claudin 11 via Src-EGFR-ERK1/2-CREB pathway in rat Sertoli cells. *Biol. Reprod.* **96**, 456-468. doi:10.1095/biolreprod.116.141267
- Raut, S., Kumar, A. V., Deshpande, S., Khambata, K. and Balasinar, N. H. (2021). Sex hormones regulate lipid metabolism in adult Sertoli cells: A genome-wide study of estrogen and androgen receptor binding sites. *J. Steroid Biochem. Mol. Biol.* **211**, 105898. doi:10.1016/j.jsbmb.2021.105898
- Setthawong, P., Phakdeedindan, P., Tiptanavattana, N., Rungarunlert, S., Techakumphu, M. and Tharasanit, T. (2019). Generation of porcine induced-pluripotent stem cells from Sertoli cells. *Theriogenology* **127**, 32-40. doi:10.1016/j.theriogenology.2018.12.033
- Shi, J.-F., Li, Y.-K., Ren, K., Xie, Y.-J., Yin, W.-D. and Mo, Z.-C. (2018). Characterization of cholesterol metabolism in Sertoli cells and spermatogenesis (Review). *Mol. Med. Rep.* **17**, 705-713. doi:10.3892/mmr.2017.8000
- Singh, A. P., Cummings, C. A., Mishina, Y. and Archer, T. K. (2013). SOX8 regulates permeability of the blood-testes barrier that affects adult male fertility in the mouse. *Biol. Reprod.* **88**, 133. doi:10.1095/biolreprod.112.107284
- Smith, L. B. and Walker, W. H. (2014). The regulation of spermatogenesis by androgens. *Semin. Cell Dev. Biol.* **30**, 2-13. doi:10.1016/j.semcdb.2014.02.012
- Stanton, P. G. (2016). Regulation of the blood-testis barrier. *Semin. Cell Dev. Biol.* **59**, 166-173. doi:10.1016/j.semcdb.2016.06.018
- Sun, T., Xin, Z., Jin, Z., Wu, Y. and Gong, Y. (2008). Effect of TGF- β /Smad signaling on sertoli cell and possible mechanism related to complete sertoli cell-only syndrome. *Mol. Cell. Biochem.* **319**, 1-7. doi:10.1007/s11010-008-9869-3
- Tanwar, P. S., Kaneko-Tarui, T., Zhang, L. H., Rani, P., Taketo, M. M. and Teixeira, J. (2010). Constitutive WNT/ β -catenin signaling in murine Sertoli cells disrupts their differentiation and ability to support spermatogenesis. *Biol. Reprod.* **82**, 422-432. doi:10.1095/biolreprod.109.079335
- Uren, P. J., Bahrami-Samani, E., de Araujo, P. R., Vogel, C., Qiao, M., Burns, S. C., Smith, A. D. and Penalva, L. O. F. (2016). High-throughput analyses of hnRNP H1 dissects its multi-functional aspect. *RNA Biol.* **13**, 400-411. doi:10.1080/15476286.2015.1138030
- Vogl, A. W., Vaid, K. S. and Guttman, J. A. (2008). The Sertoli cell cytoskeleton. *Adv. Exp. Med. Biol.* **636**, 186-211. doi:10.1007/978-0-387-09597-4_11
- Wang, B., Qi, T., Chen, S.-Q., Ye, L., Huang, Z.-S. and Li, H. (2016). RFX1 maintains testis cord integrity by regulating the expression of Itga6 in male mouse embryos. *Mol. Reprod. Dev.* **83**, 606-614. doi:10.1002/mrd.22660
- Wang, X., Wen, Y., Dong, J., Cao, C. and Yuan, S. (2018). Systematic in-depth proteomic analysis of mitochondria-associated endoplasmic reticulum membranes in mouse and human testes. *Proteomics* **18**, e1700478. doi:10.1002/pmic.201700478
- Wen, Q., Tang, E. I., Li, N., Mruk, D. D., Lee, W. M., Silvestrini, B. and Cheng, C. Y. (2018). Regulation of Blood-Testis Barrier (BTB) dynamics, role of actin-, and microtubule-based cytoskeletons. *Methods Mol. Biol.* **1748**, 229-243. doi:10.1007/978-1-4939-7698-0_16
- Wen, Y., Ma, X., Wang, X., Wang, F., Dong, J., Wu, Y., Lv, C., Liu, K., Zhang, Y., Zhang, Z. et al. (2021). hnRNPU in Sertoli cells cooperates with WT1 and is essential for testicular development by modulating transcriptional factors Sox8/9. *Theranostics* **11**, 10030-10046. doi:10.7150/thno.66819
- Willems, A., Batlouni, S. R., Esnal, A., Swinnen, J. V., Saunders, P. T. K., Sharpe, R. M., Franca, L. R., De Gendt, K. and Verhoeven, G. (2010). Selective ablation of the androgen receptor in mouse sertoli cells affects sertoli cell maturation, barrier formation and cytoskeletal development. *PLoS ONE* **5**, e14168. doi:10.1371/journal.pone.0014168
- Wong, E. W. P., Mruk, D. D., Lee, W. M. and Cheng, C. Y. (2008). Par3/Par6 polarity complex coordinates apical ectoplasmic specialization and blood-testis barrier restructuring during spermatogenesis. *Proc. Natl. Acad. Sci. USA* **105**, 9657-9662. doi:10.1073/pnas.0801527105
- Wu, Y., Guo, Q., Ju, X., Hu, Z., Xia, L., Deng, Y., Zhao, P., Zhang, M., Shao, Y., Huang, S. et al. (2021). HNRNPH1-stabilized LINC00662 promotes ovarian cancer progression by activating the GRP78/p38 pathway. *Oncogene* **40**, 4770-4782. doi:10.1038/s41388-021-01884-5
- Wu, Y., Duan, P., Wen, Y., Zhang, J., Wang, X., Dong, J., Zhao, Q., Feng, S., Lv, C., Guo, Y. et al. (2022). UHRF1 establishes crosstalk between somatic and germ cells in male reproduction. *Cell Death Dis.* **13**, 377. doi:10.1038/s41419-022-04837-2
- Xiao, R., Chen, J. Y., Liang, Z., Luo, D., Chen, G., Lu, Z. J., Chen, Y., Zhou, B., Li, H., Du, X. et al. (2019). Pervasive Chromatin-RNA binding protein interactions enable RNA-based regulation of transcription. *Cell* **178**, 107-121.e118. doi:10.1016/j.cell.2019.06.001
- Xu, H., Zhang, P., Li, R., Wu, W., Wang, S. and Xu, Y. (2018). Expression analysis of multifunctional RNA-binding protein hnRNP K during development of mammalian testis. *Pol. J. Vet. Sci.* **21**, 343-351.
- Yamazaki, T., Liu, L. and Manley, J. L. (2019). TCF3 mutually exclusive alternative splicing is controlled by long-range cooperative actions between hnRNPH1 and PTBP1. *RNA (New York, N.Y.)* **25**, 1497-1508. doi:10.1261/rna.072298.119
- Yang, Y., Jia, D., Kim, H., Abd Elmageed, Z. Y., Datta, A., Davis, R., Srivastav, S., Moroz, K., Crawford, B. E., Moparty, K. et al. (2016). Dysregulation of miR-212 promotes castration resistance through hnRNPH1-mediated regulation of AR and AR-V7: implications for racial disparity of prostate cancer. *Clin. Cancer Res.* **22**, 1744-1756. doi:10.1158/1078-0432.CCR-15-1606
- Yang, Z., Liu, Z., Yang, Y., Dai, Y. and Gao, X. (2021). Polypyrimidine tract-binding protein 1 regulates the Sertoli cell blood-testis barrier by promoting the expression of tight junction proteins. *Exp. Ther. Med.* **22**, 847. doi:10.3892/etm.2021.10279